GAIN CHARACTERISTICS OF TE CO_2 LASER AMPLIFIERS

GAIN CHARACTERISTICS OF TE CO_2 LASER AMPLIFIERS

By

CHINH DANG, B.Sc.

A Thesis

Submitted to the School of Graduate Studies

in Partial Fulfilment of the Requirements

for the Degree

Master of Science

McMaster University

August 1979

MASTER OF SCIENCE (1979) McMASTER UNIVERSITY
(Physics) Hamilton, Ontario

TITLE: Gain Characteristics of TE CO_2 Laser Amplifier

AUTHOR: Chinh Dang, B.Sc. (Université de Sherbrooke)

SUPERVISORS: Professor B.K. Garside, Professor J. Reid

NUMBER OF PAGES: xi, 88

ABSTRACT

The characteristics of small-signal gain in a TE CO_2 laser amplifier are investigated using a new technique based on gain measurements of the sequence, hot and regular CO_2 laser bands. This new technique enables us, for the first time, to determine accurately the rotational and vibrational temperatures characterizing the CO_2 laser system. The gain ratio of the sequence band to the regular band provides a simple and accurate determination of the ν_3 mode vibrational temperature. The variation of this ν_3 mode vibrational temperature with discharge energy enables us to determine the net pumping efficiency to the ν_3 mode levels as a function of input energy. It is found that the ν_3 mode vibrational temperature saturates at high input energy. This saturation sets an upper limit to the gain attainable in TE CO_2 laser amplifiers. Once this saturation occurs, increasing background gas temperature causes a reduction of gain at high input energy.

As we can measure all the characteristic temperatures relevant to the gain medium, a comparison between the calculated and experimental gain can be carried out with no adjustable parameters. The result of such a direct comparison confirms both the validity of the conventional "mode temperature" model for CO_2 laser dynamics and the validity of our measurement technique for vibrational temperatures.

The results of the present study have shown the existence of

a de-excitation mechanism occurring in the discharge, which reduces drastically the pumping efficiency to the ν_3 mode at high discharge energy. It is therefore essential to incorporate such a de-excitation mechanism in the accurate modeling of CO_2 laser dynamics. The present study contributes to a better understanding of CO_2 laser dynamics at high discharge energies.

ACKNOWLEDGEMENTS

I wish to express my deep appreciation to my supervisors, Dr. B. K. Garside and Dr. J. Reid, for their guidance and support throughout this work.

I would like to thank Dr. E. A. Ballik of McMaster University for the loan of the CW CO_2 laser cavity used in the experiment.

This work was supported, in part, by National Research Council of Canada and McMaster University.

I also want to express my many thanks to my parents for their immeasurable love.

TABLE OF CONTENTS

TABLE OF CONTENTS (Cont'd)

FIGURE CAPTIONS

FIGURE CAPTIONS (Cont'd)

FIGURE CAPITONS (Cont'd)

LIST OF TABLES

CHAPTER I

INTRODUCTION

The introduction of the transversely excited high pressure CO_2 laser in 1970 by Beaulieu [1] represented a very significant advance in high power laser technology. Recent interest in the use of CO_2 lasers as a driver for laser-induced fusion and isotope separation experiments [2,3,4] has stimulated intense work directed towards the development of high energy and high power CO_2 lasers. Detailed knowledge of the gain characteristics in CO_2 laser amplifiers plays an important role in the system design for optimal extraction of optical energy. Extensive parametric studies have been carried out in CO_2 laser amplifiers [5-10]. It was generally observed that the small-signal gain saturates rapidly as the input energy increases, and then decreases at high input energy. This gain saturation limits the extraction of energy from an amplifier.

Previous investigations of the gain characteristics were carried out by making measurements of the small-signal gain of the regular laser bands, i.e. $(00^01 - 10^00)$ and $(00^01 - 02^00)$ transitions. These measurements were made as a function of gas mixture and pressure, for several different pumping systems [5,6,7,8]. The limitation of gain was generally attributed to thermal effects such as gas temperature increase and discharge deterioration. To a large extent, discharge deterioration can be avoided by diluting CO_2 in He, by flowing the gas

mixture and by using external preionisation. Furthermore, detailed examination of the effects of gas heating on the discharge revealed that the increase of gas temperature was not sufficient to account for the observed limitation of gain, and suggested some mechanism, other than thermal effects, is involved [10].

The work reported in this thesis is aimed at a detailed study of this mechanism,which is found to be primarily responsible for the limitation of gain at high input energy in pulsed CO_2 lasers. To investigate fully the mechanism which causes gain reduction, one must be able to separately measure the population in the upper and lower laser levels. Clearly, any decrease in gain can be caused by an increase of lower laser level population, or a reduction of upper laser level population or a combination of both. Unfortunately, gain measurements of regular laser bands alone does not yield detailed information on the absolute population of laser levels, since the gain is proportional to the population difference of the laser levels. Many authors have attempted a multiple variable fit to derive the absolute population of the laser levels from gain measurements on several rotational lines of the regular bands [15,16,17,18] . However, this fitting method is insensitive to the absolute population of the levels, and is complicated by thermal effects [10,11].

In 1976, the successful laser action from high lying ν_3 mode levels (i.e., 00^02, 00^03) achieved by Reid and Siemsen [19] provided a powerful tool to investigate the dynamics of CO_2 lasers. These new laser bands are named "sequence bands". The gain ratio of the first

sequence band ($00^{0}2$) to the regular band ($00^{0}1$) depends only on the ν_3 mode vibrational temperature [20]. Measurement of this gain ratio enables us to monitor the discharge excitation to the ν_3 mode independent of thermal effects, and to accurately determine the ν_3 mode vibrational temperature. A knowledge of this vibrational temperature enables us to calculate the absolute population in the vibrational levels, and to investigate the fundamental mechanisms which limit the gain in a TE CO_2 laser amplifier. The most important outcome of the present study is the discovery that the ν_3 mode vibrational temperature saturates at high input energy. It is this saturation which sets a fundamental limitation to the gain attainable in a TE CO_2 laser amplifier. We interpret the saturation of the ν_3 mode vibrational temperature as being caused by a de-excitation mechanism which occurs during the discharge, possibly electron de-excitation of excited states [21,22].

In Chapter IV, strong experimental evidence is presented to show clearly the saturation of ν_3 mode vibrational temperature at high input energy. A study of the dependence of the ν_3 mode vibrational temperature on gas mixture shows substantial differences between the behavior of N_2 and CO_2 in a glow discharge, and reveals another reason for the importance of N_2 in CO_2 lasers.

In Chapter V, we compare experimental gain data to the values calculated from a conventional "three temperatures" model (as described in Section II-4-5) with no adjustable parameters. Such a direct comparison is performed for the first time, since previous researchers could not measure the vibrational temperatures, and hence used them

as variable parameters. This direct comparison of theory and experiment produces good agreement over a wide range of gas mixture and input energy, confirming the validity of both the conventional "mode temperature" model for CO_2 laser dynamics, and our measurement technique of vibrational temperatures.

All measurements described in this thesis were made using a pin-pin resistive discharge at a fixed pressure of 92 torr. This moderate pressure and simple discharge system are chosen to ensure a stable discharge over a wide range of gas mixtures. The maximum input energy per unit volume per unit pressure used in this series of experiments is much greater than that used in the most powerful TE lasers. As previous research has shown that the dependence of gain on input energy does not change with pressure, the conclusions reached from the present study also apply to the most up-to-date, high pressure TE CO_2 lasers. It is hoped that this work will make a significant contribution to the better understanding of TE CO_2 laser dynamics.

CHAPTER II

THEORY [24]

This chapter begins with a brief look at the CO_2 molecular structure and its energy level diagram, with emphasis on the levels involved in the laser transitions. Then, a theoretical model which relates the small-signal gain to various parameters and molecular constants is described in detail, together with all the assumptions made. A comparison is made between the available data on the molecular constants, and a best choice of the values is used in the calculations. Finally, the model is applied to derive several important relationships appropriate to the experiment. These relationships are used to make comparison between theory and experiment as given in Chapter V.

II-1 CO_2 molecular structure

The $C^{12}O_2^{16}$ molecule is a triatomic linear molecule belonging to the point group $D_{\infty h}$, i.e., it possesses an axis of symmetry C_∞, and a plane of symmetry perpendicular to the C_∞ axis. The equilibrium nuclear distance of the C=O bond in the electronic ground state $^1\Sigma_g^+$ is $r_e = 1.1615 \times 10^{-8}$ cm [25]. There are three nomal modes of vibration, namely, symmetric stretching ν_1, bending ν_2 and asymmetric stretching ν_3, which are associated with the species Σ_g^+, π_u and Σ_u^+, respectively. A classical schematic representation of the three modes is given in Fig. 1.

FIGURE 1

The three normal modes of vibration of the CO_2 molecule.

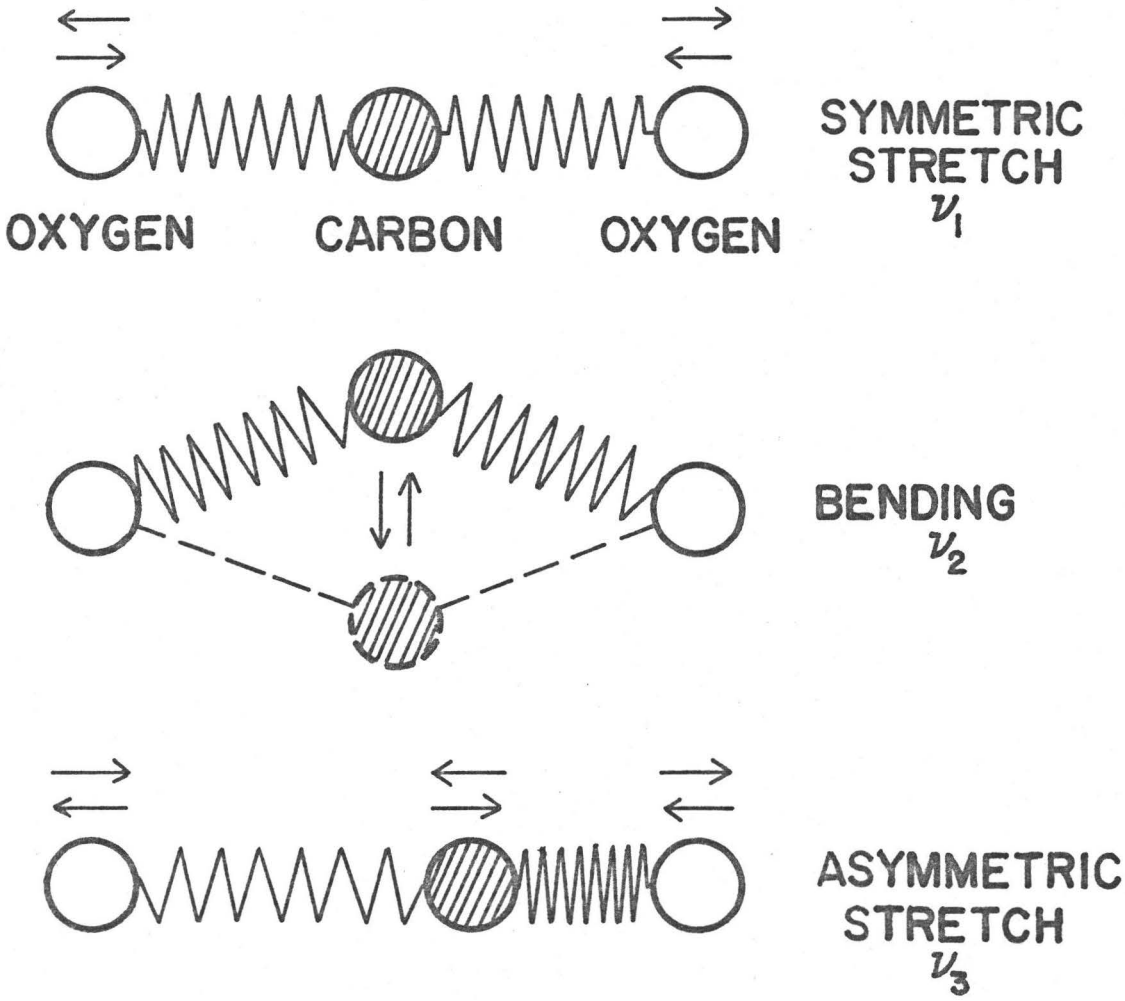
OXYGEN
CARBON
OXYGEN
SYMMETRIC STRETCH
ν_1
BENDING
ν_2
ASYMMETRIC STRETCH
ν_3

II-2 Energy diagram

The spectroscopy of the CO_2 molecule is well understood [25]. Due to the symmetry of the molecule and the spinless nuclei, the anti-symmetric rotational levels are missing entirely. This produces a alternate spectrum in the $\Sigma_u^+ - \Sigma_g^+$ vibro-rotational laser transitions (see Fig. 2). In the present context, only those vibro-rotational levels of the electronic ground state relevant to the laser radiation are of interest, therefore only those vibrational levels involved in the laser transitions are featured in the energy diagram presented in Fig. 3. In the same figure, some low lying vibrational levels of the N_2 molecule are also indicated. These play a role of primary importance in the high efficiency of the CO_2 lasers. Each vibrational level of the CO_2 molecule is identified by a set of four quantum numbers $(\nu_1 \nu_2^{\ell} \nu_3)$ where ν_1, ν_2, ν_3 are the vibrational quantum numbers associated with the ν_1, ν_2, ν_3 modes respectively, and ℓ is an angular momentum quantum number (see below). In the harmonic approximation, the CO_2 molecule is treated as a combination of three independent harmonic oscillators, with the second vibrational mode being doubly degenerate. This degeneracy is partly removed by considering the anharmonicity which is equivalent to introducing an angular momentum with quantum number $\ell = \nu_2, \nu_2 - 2, \ldots, 1$ or 0 depending on whether ν_2 is odd or even [25]. Each non-zero ℓ has a two-fold degeneracy on account of the equivalence of the two directions of the angular momentum, this ℓ-type doubling can be removed by increasing rotation as a result of the coriolis force. Thus, for each rotational quantum number J, a

FIGURE 2

Symmetry properties of the rotational levels in various species of vibrational levels of CO_2 molecule. The dashed lines represent the missing antisymmetric rotational levels. As an example, the levels $(02^{o}0)$ and $(10^{o}0)$ are of specie Σ_g^+ and the level $(00^{o}1)$ is of specie Σ_u^+. The laser transitions $(00^{o}1 - 02^{o}0)$ and $(00^{o}1 - 10^{o}0)$ exist only between the odd J levels of $(00^{o}1)$ and the even J levels of $(02^{o}0)$ and $(10^{o}0)$.

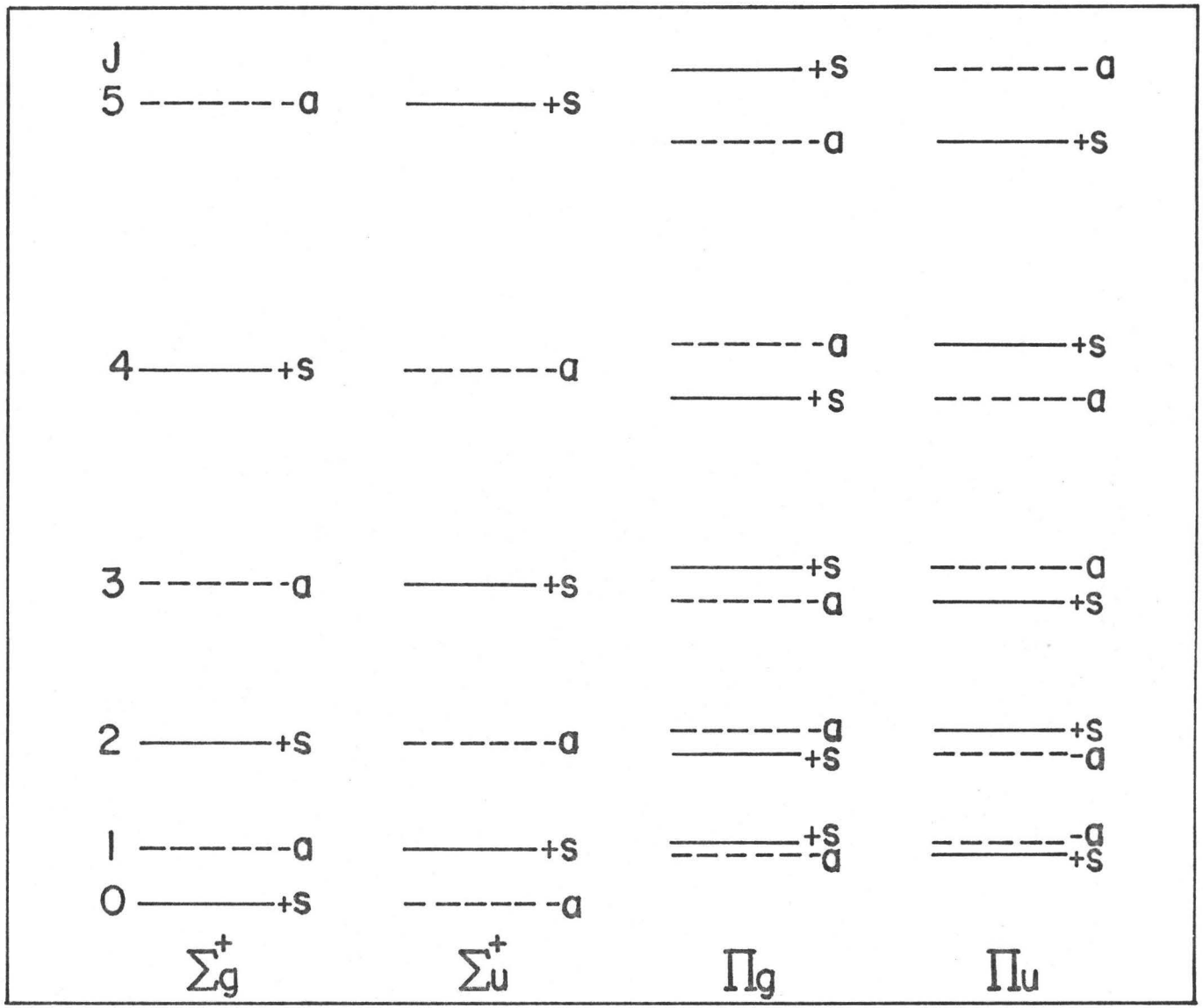
J
5
4
3
2
1
0
-a
+s
Σ_g^+
Σ_u^+
Π_g
Π_u

FIGURE 3

Energy diagram of the vibrational levels in the electronic ground state of the CO_2 molecule. The laser transitions are indicated by the arrowed lines. The dashed arrowed lines indicate weak transitions which have not yet been observed to lase. Some vibrational levels of N_2 are also shown.

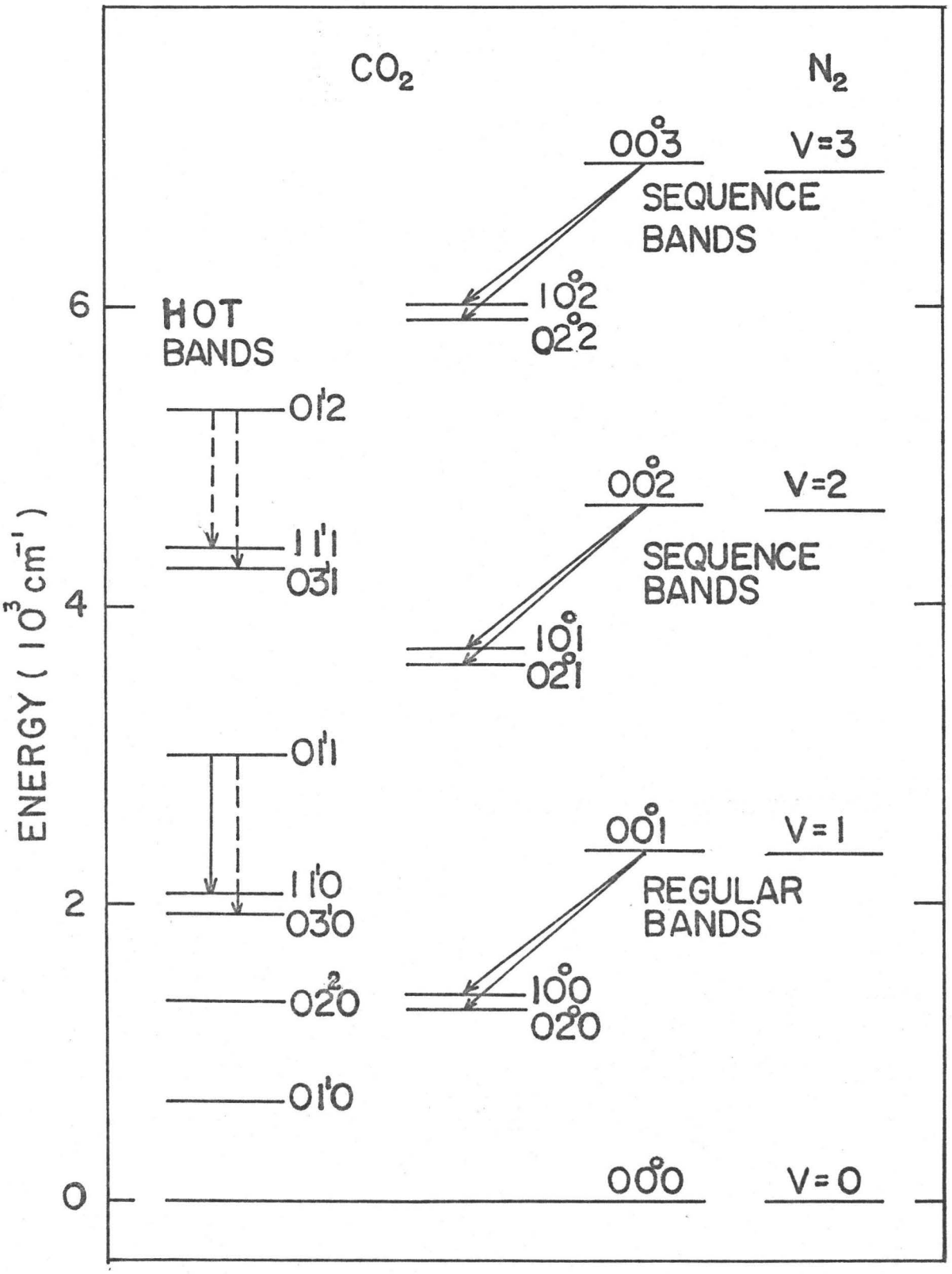
CO2
N2
00°3
V=3
SEQUENCE
BANDS
10°2
02°2
HOT
BANDS
01'2
00°2
V=2
11'1
03'1
SEQUENCE
BANDS
10°1
02°1
01'1
00°1
V=1
11'0
03'0
REGULAR
BANDS
02'0
10°0
02°0
01'0
00°0
V=0
ENERGY (10^3 cm^-1)
6
4
2
0

splitting into two components occurs whose separation increases with increasing J where J = ℓ, ℓ + 1, ℓ + 2, ..., etc. This phenomenon is illustrated in Fig. 2 [25].

There is an important perturbation which causes a large energy shift of some of the vibrational levels in the CO_2 molecule. This is called Fermi resonance [25], and occurs between vibrational levels of the same specie lying very close together. The Fermi shift occurs in the CO_2 molecule between the ν_1 and ν_2 modes due to the accidental coincidence of the vibrational frequencies, i.e., $\nu_1 \simeq 2\nu_2$. The energy level shift is included in the energy levels shown in Fig. 3. This strong Fermi resonance between the ν_1 and ν_2 modes has an important consequence in the relaxation processes of the laser system (see Section II-4-5).

The energy (in cm^{-1}) of a vibro-rotational level in CO_2 is given by:

$$E(v_1 v_2^{\ell} v_3; J) = G_v(v_1 v_2^{\ell} v_3) + F_v(J) \qquad (1)$$

where G_v is the vibrational energy and F_v is the rotational energy. The subscript v is used to indicate the dependence on the vibrational level. The vibrational energy is:

$$E_v(v_1 v_2^{\ell} v_3) = \sum_{i=1}^{3} \nu_i\left(v_i + \frac{d_i}{2}\right) + \sum_i \sum_k X_{ik}\left(v_i + \frac{d_i}{2}\right)\left(v_k + \frac{d_k}{2}\right) + g\ell^2 \qquad (2)$$

where d_i = 1 for nondegenerate and 2 for doubly degenerate vibrations. The first summation in Eq. (2) is the dominant one; the double sum

gives the higher-order correction terms which arise from cross coupling between different modes of vibration through the anharmonic force constants X_{ik}. The last term is the ℓ-type doubling contribution where g has the same order of magnitude as the constants X_{ik}. For instance, as $G_v(00^0 1) = 2349\ cm^{-1}$ and $G_v(00^0 2) = 4673\ cm^{-1}$ the anharmonicity effect is seen to be small.

The rotational energy is:

$$F_v(J) = B_v J(J+1) - D_v J^2(J+1)^2 + H_v J^3(J+1)^3 + \ldots \qquad (3)$$

where B_v is the rotational constant at the specific vibrational level, and D_v, H_v are the higher order corrections which are small compared to B_v (In CO_2, $B_v \sim .38\ cm^{-1}$, $D_v \sim 10^{-7}\ cm^{-1}$ and $H_v \sim 10^{-14}\ cm^{-1}$).

II-3 Selection rules and the laser transitions

The selection rules for vibrational-rotational transitions in the IR spectrum are [26] :

$\Delta\ell = 0, \pm 1, \quad \Sigma^+ \leftrightarrow \Sigma^-, \qquad g \not\leftrightarrow g, \qquad u \not\leftrightarrow u$

$\Delta\ell = 0, \pm 1, \ (J=0) \not\leftrightarrow (J=0), \qquad + \leftrightarrow -, \qquad s \leftrightarrow a$

where s and a designate the symmetric and antisymmetric, and the symbols $\leftrightarrow$ and $\not\leftrightarrow$ represent "allowed" and "not allowed", respectively.

Two strong CO_2 laser transition bands were observed early in 1964 by Patel [27]. These transitions were found to be $\Sigma_u^+ - \Sigma_g^+$ vibrational bands $(00^0 1 - 10^0 0)$ and $(00^0 1 - 02^0 0)$[28] with band centres at 10.4 μm and 9.4 μm, respectively. Laser transitions were obtained from both the P branch ($\Delta J = -1$) and the R branch ($\Delta J = +1$) of each band.

The Q branch ($\Delta J = 0$) is not allowed because transitions can not occur between two Σ - states for which $\ell = 0$. Figure 4 gives a detailed transition diagram for laser oscillations from both the P and R branches of the $00^0 1 - 10^0 0$ and $00^0 1 - 02^0 0$ bands. These two laser bands share the common upper level $00^0 1$ which is the first excited ν_3 mode vibrational level. Also, a much weaker laser band, namely, the 10.8 μm $01^1 1 - 11^1 0$ "hot band" has been observed and is responsible for the intensity anomalies [29] observed in several lines of the regular laser transitions. Note that the 9.3 μm $01^1 1 - 03^1 0$ hot band overlaps the 9.4 μm $00^0 1 - 02^0 0$ regular band, and has never been observed to lase.

Recently, many new laser transitions [19] were discovered in a CO_2 laser using an in-cavity hot cell [31] to suppress the strong regular laser transitions. These new laser transitions, involving higher ν_3 mode vibrational levels, are the 10.4 μm $00^0 2 - 10^0 1$, 9.3 μm $00^0 2 - 02^0 1$, 10.4 μm $00^0 3 - 10^0 2$ and 9.3 μm $00^0 3 - 02^0 2$ bands. The lower laser levels have the usual Fermi mixing as the $10^0 1$ and $02^0 0$ levels. These new laser transitions provide a powerful tool to investigate the characteristics of CO_2 lasers. This will be discussed in the following sections. The spectra of the 9.4 μm $00^0 1$ and 9.3 μm $00^0 2$ laser bands are shown in Fig. 5.

II-4 Relationship between small-signal gain and population inversion

To obtain an accurate knowledge of any laser system, it is important to be able to relate gain coefficient [32] to population

FIGURE 4

Detailed transition diagram of laser oscillations in the 10.4 μm and 9.4 μm regular bands (from reference 26).

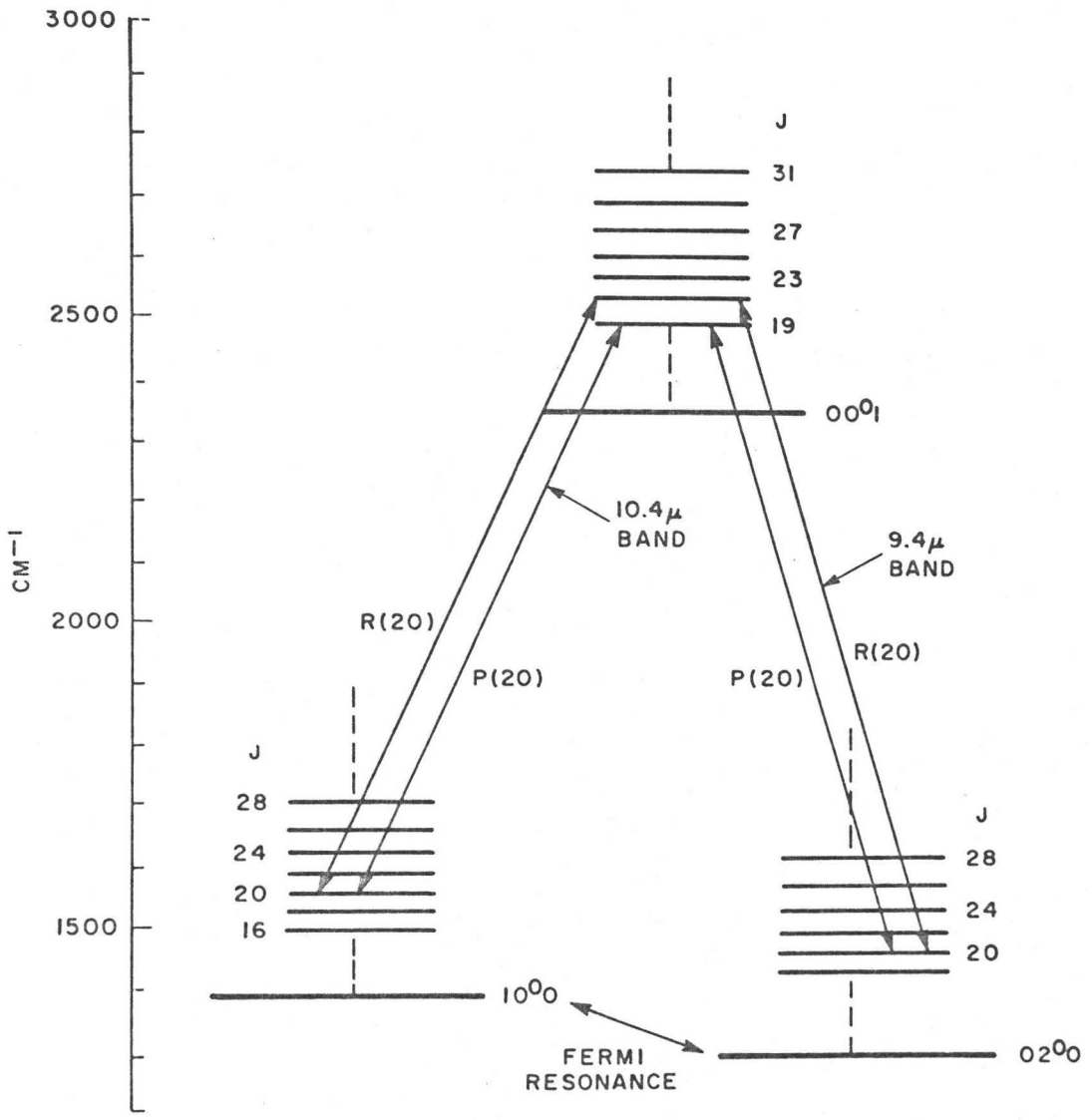
3000
2500
2000
1500
CM⁻¹
J
31
27
23
19
00⁰1
10.4μ BAND
9.4μ BAND
R(20)
P(20)
P(20)
R(20)
J
28
24
20
16
10⁰0
J
28
24
20
FERMI RESONANCE
02⁰0

FIGURE 5

Calculated relative gain versus wavenumber for the 9.4 μm $00^{0}1$ and $00^{0}2$ bands in CO_2 for typical discharge conditions. For sake of clarity, the sequence gain is shown negative.

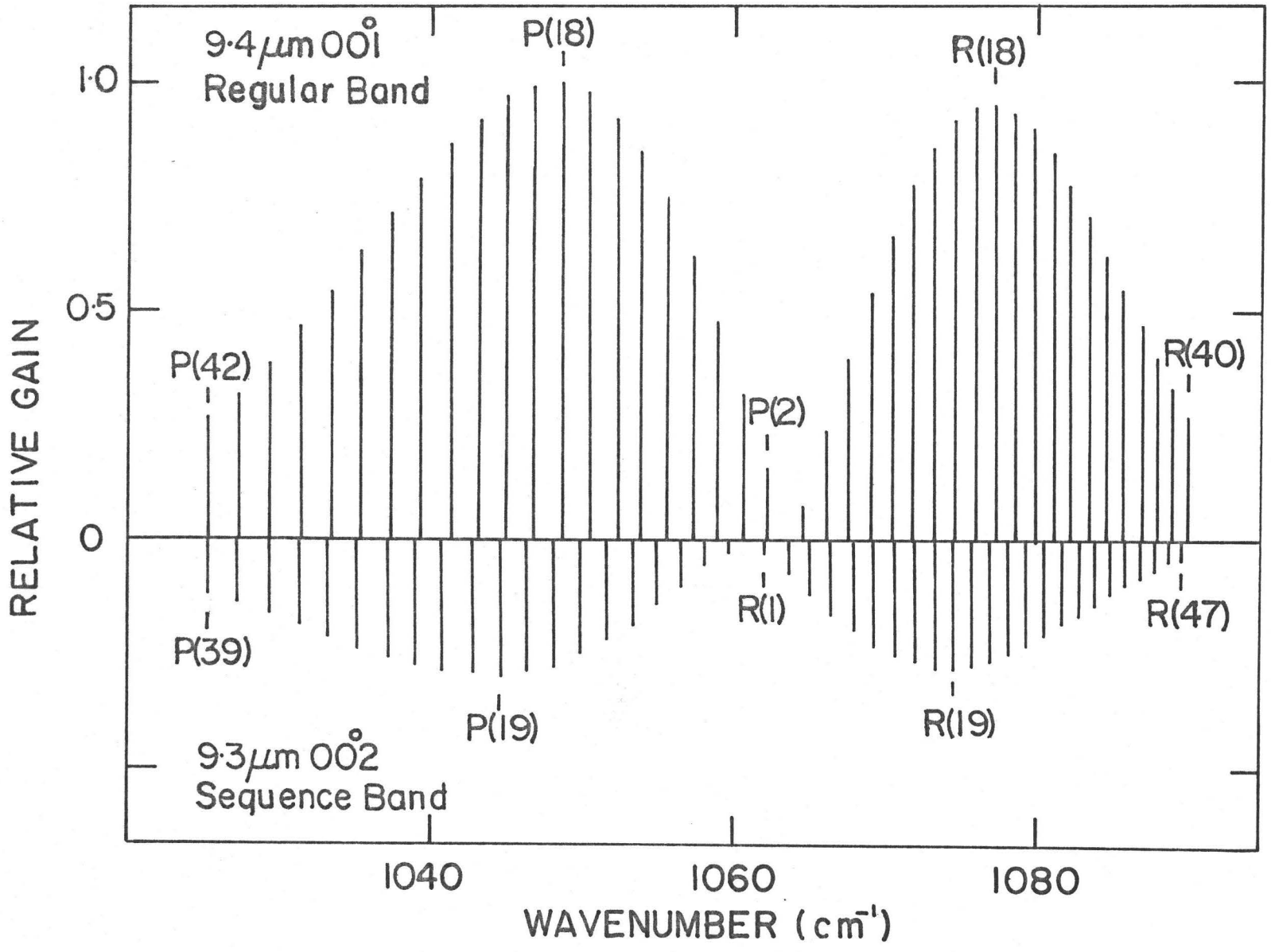
9·4μm 00°1
Regular Band
P(18)
R(18)
1·0
0·5
0
RELATIVE GAIN
P(42)
P(2)
R(40)
P(39)
R(1)
R(47)
P(19)
R(19)
9·3μm 00°2
Sequence Band
1040
1060
1080
WAVENUMBER (cm⁻¹)

inversion. The situation in CO_2 is somewhat complicated by the large number of rotational levels, and consequently a detailed calculation is presented below.

In a gas, the gain coefficient between two levels, u (upper) and ℓ(lower) can be written as [33]:

$$\alpha(\nu) = \frac{\lambda_o^2}{8\pi} A_{u\ell} \left[N_u - \frac{g_u}{g_\ell} N_\ell\right] g(\nu) \qquad (4)$$

where λ_o is the wavelength at the center of the spectral line, $A_{u\ell}$ is the spontaneous transition probability, N_u and N_ℓ are population densities of the upper and lower levels having statistical weights g_u and g_ℓ, and $g(\nu)$ is the normalised lineshape function evaluated at the frequency ν. In the following subsections, we will examine in detail all the parameters appearing in Eq. (4).

II-4.1 Wavelength at line center

The wavelength of the laser transitions is well known and is measured with very high accuracy (one part in 10^8 cm^{-1}) by heterodyning two stable CW CO_2 lasers [34]. For the computational purposes, we use the data of Dupre-Maquaire *et al.* [35].

II-4.2 Spontaneous transition probability

The spontaneous transition probability can be written as[33]:

$$A_{u\ell} = \frac{64\ \pi^4}{3h\lambda_o^3} \quad \frac{|R_\ell^u|^2 S_J F_J}{g_u} \qquad (5)$$

where $|R_\ell^u|^2$ is the vibrational contribution to the transition moment, S_J is the rotational contribution and F_J is the interaction factor

between vibration and rotation.

The values of S_J for transitions between different species of vibrational levels are given in Reference [36]. Values relevant to the laser transitions are reproduced in Table I. The statistical weight g_u of a rotational level J_u for $C^{12}O_2^{16}$ is $2J_u + 1$.

The determination of $|R_\ell^u|^2$ and F_J is inherently related to the lineshape function $g(\nu)$ and will therefore be discussed in the next subsection.

II-4.3 Normalized lineshape function

The normalized lineshape function for combined Doppler and collision broadening is given by [33]:

$$g(\nu) = \frac{1}{\pi^{3/2}\Delta\nu_c} \int_{-\infty}^{\infty} \frac{a^2 e^{-t^2} dt}{a^2 + (\omega - t)^2} \qquad (6)$$

where $a = \frac{\Delta\nu_c}{\Delta\nu_D} (\ln 2)^{\frac{1}{2}}$; $\omega = \frac{(\nu - \nu_o)}{\Delta\nu_c} a$ with $\Delta\nu_D$ and $\Delta\nu_c$ the Doppler and collision linewidths (Half Width at Half Maximum).

At line center, $\nu = \nu_o$, Eq. (6) can be reduced to:

$$g(\nu_o) = \frac{1}{\pi^{\frac{1}{2}} \Delta\nu_c} a e^{+a^2} \operatorname{erfc}(a) \qquad (7)$$

The Doppler line width (HWHM) is calculated from:

$$\Delta\nu_D = \frac{\nu_o}{c} \left(2 \frac{k_B T}{M} \ln 2\right)^{\frac{1}{2}} \qquad (8)$$

where c is the velocity of light; k_B is the Boltzmann constant; T is the absolute gas temperature, and M is the mass of the lasing molecule (i.e., CO_2).

In addition to its linear pressure dependence, the collision linewidth varies also with the composition of the gas mixture and the laser line under consideration. Following the notation of Patty et al. [37], this can be written as:

$$\Delta\nu_c(J) = \frac{C_{CO_2}(J)}{T^{\frac{1}{2}}}\left[P_{CO_2} + \frac{P_b}{B_{CO_2,b}} + \frac{P_c}{B_{CO_2,c}} + \ldots\right] \qquad (9)$$

where P_i is the partial pressure of gas componant i and the constants $B_{CO_2,i}$ and C_{CO_2} are related to the optical broadening cross section as defined in the above reference.

Equation (9) indicates that $\Delta\nu_c$ is proportional to $T^{-\frac{1}{2}}$ [74]. However, Ely and McCubbin suggest that $\Delta\nu_c$ varies more closely as T^{-1} in the range 300 - 400 K [38]. Most recent work by Robinson et al. [39] and Miller et al. [40] favor the temperature dependence $T^{-\frac{1}{2}}$, and hence we choose $\Delta\nu_c \propto T^{-\frac{1}{2}}$ in our calculations. As the majority of our experimental results deal with T in the range from 300 to 400 K, the difference in the two formulations is small.

The constants $B_{CO_2,i}$, C_{CO_2}, F_J and $|R_\ell^u|^2$ for the 00^0l regular bands have been determined by many authors [41,42,43]. The usual method consists of measuring the absorption on many rotational (laser) lines in pure CO_2 gas, and in mixtures with He and N_2, at low (~5 torr) and high (>100 torr) pressures, at room temperature. Good agreement (within 5%) is generally obtained between different measurements of absorption at high pressure, but at low pressure (due to the smaller absorption coefficient, the measurement is more difficult) the scatter between

measurements is larger. This directly affects the values of $B_{CO_2,i}$, C_{CO_2}, F_J and $|R_\ell^u|^2$, which are deduced from a combination of the low and high pressure absorption measurements.

The most recent determination of the constants $B_{CO_2,i}$ and C_{CO_2} was by R.L. Abrams [44] using a tunable CO_2 laser to measure directly the linewidth. These results are inherently more accurate since they do not depend upon F_J and $|R_\ell^u|^2$. Unfortunately, only one line, the 10.4 μm $00^0 1$ P(20), was measured, and the J dependence of C_{CO_2} was not determined. Nevertheless, the accurate values of $B_{CO_2,i}$ can be used in calculation for gas mixtures, as there is only a weak dependence upon the rotational lines and the laser bands [45].

The vibration-rotation interaction factor F_J is not widely determined because its value is nearly unity. The available data for the $00^0 1$ bands are taken from the results of Cousin et al. [42].

As mentioned above, the values of the constants C_{CO_2} and $|R_\ell^u|^2$ deduced individually from the absorption measurements are not in such good agreement as the absorption coefficients at high pressure. Therefore we have chosen a set of values from the same author to ensure consistency in the calculation. The values of the different constants used in the computation of gain coefficients for the $00^0 1$ regular bands are summarized in Table I.

For the $00^0 2$ sequence bands, diode laser measurements of CO_2 by Reid et al. [46] show that the 9.4 μm $00^0 2$ and $00^0 1$ bands have identical linewidth within experimental error, and that the ratio of the square of the matrix elements for the two 9.4 μm bands $(R_{02^0 1}^{00^0 2}/R_{02^0 0}^{00^0 1})^2$

TABLE I

VALUE OF THE CONSTANTS USED IN THE GAIN CALCULATIONS

Laser Band	S_J for P branch (a)	F_J for P branch	$\lvert R_\ell^u \rvert^2$ [c.g.s.]	$\frac{\lvert R_\ell^u \rvert^2}{\lvert R^{00^0 1} \rvert^2}$	$\Delta\nu_c(J)$ for P branch [MHz]
$00^0 1\text{-}10^0 0$	J_ℓ	$1+0.0009J_\ell-0.00006J_\ell^2$ (b)	4.01×10^{-20} (b)		$\frac{90.05-0.8791J_\ell}{T^{\frac{1}{2}}} \times\left[P_{CO_2}+\frac{P_{N_2}}{1.36}+\frac{P_{He}}{1.56}\right]$ (b)(d)
$01^1 1\text{-}11^1 0$	$\frac{2(J_\ell^2-1)}{J_\ell}$	"		0.54 (e)	"
$00^0 1\text{-}02^0 0$	J_ℓ	$1+0.0005J_\ell+0.00008J_\ell^2$ (c)	3.40×10^{-20} (c)		$\frac{77.94-0.5333J_\ell}{T^{\frac{1}{2}}} \times\left[P_{CO_2}+\frac{P_{N_2}}{1.36}+\frac{P_{He}}{1.56}\right]$ (c)(d)
$00^0 2\text{-}02^0 1$	J_ℓ	"		1.89(f)	"

(a) Penner[36], (b) Arie [42], (c) Cousin [41], (d) Abrams [44], (e) Rothman [48], (f) Reid [46].

is measured as 1.89 $\pm$ 0.12. Moreover, based on extensive gain measurements in both 10.4 μm and 9.4 μm regular and sequence bands over a wide range of discharge conditions, it has been determined that the ratio $(R^{00^02}_{10^01}/R^{00^01}_{02^01})^2$ is 2.10$\pm$0.17 for the corresponding 10.4 μm bands [47]. Hence the average value of $(R^{00^02}/R^{00^01})^2$ in both 10.4 μm and 9.4 μm bands is very close to 2.0, with a slight shift of band strength in favor of the 10.4 μm 00^02 bands. This average value is in good agreement with the harmonic oscillator model of CO_2, which predicts that the ratio should be exactly equal to 2.

Similar behavior is expected for the (01^11) hot bands. Therefore, we assume that the linewidth is the same for the (00^01) regular bands and (01^11) hot bands. Also, from the band intensities data compiled by Rothman *et al.* [48], it is found that the ratios $(R^{01^11}_{11^10}/R^{00^01}_{10^00})^2$ and $(R^{01^11}_{03^10}/R^{00^01}_{02^00})^2$ are 0.54 and 0.49 respectively. This agrees well with the prediction of the harmonic oscillator model of CO_2, which gives a value of 0.5 on account of the two-fold degeneracy of the hot bands.

II-4.4 Population density for absorption

If thermal equilibrium is established between all degrees of freedom in a gas, its state is specified by a single gas temperature and pressure. Under the assumption that the harmonic oscillator approximation is valid, and the Fermi resonance, the vibro-rotational interaction, and the ℓ-doubling are negligible, the CO_2 molecules can be treated as a gas of three independent rigid-rotor harmonic oscillators.

According to Gray and Selvidge [49], these simplifications result in errors less than 2% in the computation of the internal partition function [50] for temperatures up to 1200°K. Thus, the internal partition function Q_{int} of the system can be factorized into two terms, i.e.:

$$Q_{int} = Q_V \cdot Q_R \tag{10}$$

where Q_V is the vibrational partition function and Q_R is the rotational partition function.

The vibrational partition function is calculated from [33]:

$$Q_V = \sum_i^3 \sum_{v_i}^{\infty} g_{v_i} \exp\left[-E_V(v_i)/k_B T\right]$$

$$= \left[(1-e^{-h\nu_1/k_B T})(1-e^{-h\nu_2/k_B T})^2(1-e^{-h\nu_2/k_B T})\right]^{-1} \tag{11}$$

where the vibration frequencies ν_1, ν_2 and ν_3 are the perturbed values of the three normal vibration modes of CO_2, namely,

$$\nu_1/c = 1388.1881 \text{ cm}^{-1};\ \nu_2/c = 667.3807 \text{ cm}^{-1};$$

$$\nu_3/c = 2349.1467 \text{ cm}^{-1}$$

The rotational partition function is calculated from [33]:

$$Q_R = \sum_J g_J \exp\left[-F_V(J)/k_B T\right]$$

$$= \sum_J (2J+1) \exp\left[-B_V J(J+1)/k_B T\right] \tag{12}$$

where the summation is over the rotational quantum number J which can be all even or all odd for $\ell = 0$ or all interger for $\ell \neq 0$ depending on the vibrational level. B_V is the rotational molecular constant of the vibrational level under consideration. The higher order corrections in $F_V(J)$ are neglected.

By transforming the summation to an integral, we obtain:

$$Q_R = \begin{cases} \dfrac{k_B T}{2B_v hc} & \text{for summation over even or odd J} \\ \dfrac{k_B T}{B_v hc} & \text{for summation over all J} \end{cases}$$

Now that the internal partition function has been calculated, the population density N_{vJ} of any vibro-rotational level can be obtained from:

$$N_{vJ} = N \frac{g_v g_J \exp\left[-E(v,J)/k_B T\right]}{Q_V \cdot Q_R} \qquad (14)$$

where N is the total number density of CO_2 molecules; g_v, g_J are the statistical weights of the vibrational and rotational levels; and E(v,J) is the perturbed vibro-rotational energy calculated from Eq.(1).

By combining Eqs. (1)-(14), we are able to calculate the absorption coefficient [51] of any CO_2 gas mixture, and good agreement is obtained with experimental results (see Table II). However, this simple calculation can only be applied to the absorption coefficient where the gas is in thermal equilibrium. In a gain medium, a population inversion is essential, i.e. $N_u > N_\ell$, hence a non-thermal equilibrium must exist. This complicated situation is controlled by many processes: relaxations, excitations and de-excitations between electrons, ions, molecules and photons. These processes are the subject of many theoretical and experimental studies. Extensive research has been carried out into CO_2 laser dynamics, and the basics mechanisms in the laser are now fairly well understood. The most successful model is based

TABLE II

ABSORPTION COEFFICIENT IN PURE CO_2 AT P = 100 torr AND T= 300 K

Line		$-\alpha(\nu_o) \times 10^3$ cm^{-1} Computed	Experimental
10.4 μm $00^0 1$	P(10)	1.48	1.46[a]
	P(14)	1.79	1.81
	P(18)	1.87	1.87
	P(22)	1.75	1.74
	P(26)	1.49	1.44
9.4 μm $00^0 1$	P(10)	2.19	2.30[b]
	P(14)	2.64	2.65
	P(18)	2.76	2.75
	P(24)	2.42	2.40
	P(28)	1.99	2.04

(a) Arie, et al. [42]

(b) Cousin, et al. [41]

on the theory of local equilibrium vibrational temperature [52], which will be described in detail in the next subsection and will be used throughout this thesis.

II-4.5 Model for population inversion calculations

The local equilibrium vibrational temperature was first introduced by Gordietz et al.[52] in an attempt to model the CO_2 laser. The main simplifying assumption in this model is that a single vibrational temperature can be introduced for each vibrational mode. This mode temperature approach has been applied successfully by Moore [53], Tulip [54], Seguin [55] and many others for accurate modeling of the CO_2 laser. This model is successful because the intramode V-V energy exchange rate in CO_2 is much faster than the intermode V-V energy transfer rate, and the V-T energy transfer rate. Therefore, in each mode of vibration, a Boltzmann distribution is established with a characteristic vibrational temperature.

Hocker et al. [56] have shown experimentally that the levels (00^0n) for n = 1 to 4, are strongly coupled by collisions with a fast rate $\sim 10^5$ $sec^{-1}torr^{-1}$. The near-resonant V-V intramode energy transfer processes such as:

$$2\ CO_2(00^01) \rightleftharpoons CO_2(00^02) + CO_2(00^00) + 25\ cm^{-1} \qquad (15)$$

are presumed to be responsible for this. The symmetric stretching and bending levels are also expected to be in rapid equilibrium within each mode due to similar near-resonant processes:

$$2\ CO_2(10^0 0) \rightleftharpoons CO_2(20^0 0) + CO_2(00^0 0) - 21\ cm^{-1} \quad (16)$$

$$2\ CO_2(01^1 0) \rightleftharpoons CO_2(02^0 0) + CO_2(00^0 0) + 49\ cm^{-1} \quad (17)$$

$$2\ CO_2(01^1 0) \rightleftharpoons CO_2(02^2 0) + CO_2(00^0 0) - 1\ cm^{-1} \quad (18)$$

These processes (15)-(18) are sufficiently fast to ensure a single temperature for each vibrational mode of the CO_2 modelcule.

The intermode V-V rates of processes such as:

$$CO_2(00^0 1) + CO_2(00^0 0) \rightleftharpoons CO_2(v_1 v_2^{\ell} 0) + CO_2(00^0 0) + \text{K.E.} \quad (19)$$

$$CO_2(10^0 0) + CO_2(00^0 0) \rightleftharpoons CO_2(02^0 0) + CO_2(00^0 0) + 103\ cm^{-1} \quad (20)$$

have also been measured. The rate of process (19) is slow, ~ 350 sec^{-1} $torr^{-1}$ at room temperature [57]. However, due to the strong coupling by Fermi resonance, the rate for process (20) is expected to be fast, ~10^5 sec^{-1} $torr^{-1}$ [59,60]. On the other hand, some experiments [58] do appear to indicate that the coupling between the two modes is not so strong ($\lesssim 10^4$ sec^{-1} $torr^{-1}$). A direct consequence of this disagreement is: if the coupling is strong, the ν_1 and ν_2 modes will have same vibrational temperature; whereas, if the coupling is weak, each mode will have its own vibrational temperature. For the present study where we are working in the 9.4 μm laser bands, this distinction is not important, and the two modes are taken to have the same temperature (see also discussions in Chapter V).

Furthermore, the relaxation rate of the rotational levels is measured to be very fast, ~10^7 sec^{-1} $torr^{-1}$ [61]. We therefore assume that the rotational level distribution is in equilibrium with the gas

kinetic temperature.

In addition to the self relaxation of the CO_2 molecule, gas components such as He and N_2 play an important role in the laser dynamics. Due to its high heat conductivity, He lowers the gas temperature, and by redistributing the local heating, it reduces the occurrence of local arcing [26]. It is also believed that He is effective in relaxing the lower laser levels, with a rate ~3×10^3 $sec^{-1}torr^{-1}$ through the V-T process [64]:

$$CO_2(01'0) + He \longrightarrow CO_2(00^0 0) + He + 667\ cm^{-1} \qquad (21)$$

It is well known that the vibrational energy levels of the electronic ground state of the N_2 molecule are in near-resonance with the ν_3 mode energy levels of CO_2. This ensures a very fast V-V energy transfer rate, ~10^4 sec^{-1} $torr^{-1}$ [57] by processes such as:

$$CO_2(00^0 1) + N_2(0) \rightleftarrows CO_2(00^0 0) + N_2(1) + 19\ cm^{-1} \qquad (22)$$

Moreover, as the vibrational levels of N_2 have a very long lifetime, the N_2 molecules act as an energy reservoir for the ν_3 mode CO_2 molecules.

In summary, processes such as (22) ensure a common vibrational temperature for the N_2 and the ν_3 mode CO_2 molecules; also, processes such as (15)-(18) ensure a mode temperature for each vibrational mode of the CO_2 molecule. Finally, the rotational temperature is taken to be in equilibrium with the gas temperature due to fast rotational relaxation. Consequently, we require only three temperatures, namely, the rotational temperature T_R, the ν_1(or ν_2) mode vibrational temperature $T_1(=T_2)$, and the ν_3-mode vibrational temperature T_3, to specify the

molecular populations in the CO_2-N_2-He laser.

It is now straightforward to incorporate these three temperatures T_R, T_2 and T_3 in the small-signal gain calculation. Equation (11) will be replaced by:

$$Q_v = [(1-e^{-h\nu_1/k_BT_2})(1-e^{-h\nu_2/k_BT_2})^2(1-e^{-h\nu_3/k_BT_3})]^{-1} \qquad (23)$$

The expression (13) for the rotational partition function will stay unchanged since the rotational temperature T_R is identical to the gas temperature T.

In the harmonic oscillator approximation, the population density of any vibrational level $(v_1 v_2^{\ell} v_3)$ is given by:

$$N(v_1 v_2^{\ell} v_3) = N \frac{(g_{v_1} e^{-v_1 h\nu_1/k_BT_2})(g_{v_2} e^{-v_2 h\nu_2/k_BT_2})(g_{v_3} e^{-v_3 h\nu_3/k_BT_3})}{Q_V}$$

where g_{v_1}, g_{v_2} and g_{v_3} are the statistical weights of the vibrational level and N is the total number density of CO_2 molecule.

Let us define the quantities $x_i = \exp(-h\nu_i/k_BT_i)$, i = 1,2,3. The population density of $(v_1 v_2^{\ell} v_3)$ can be rewritten as:

$$N(v_1 v_2^{\ell} v_3) = N \frac{g_{v_1} g_{v_2} g_{v_3} x_1^{v_1} x_2^{v_2} x_3^{v_3}}{Q_V} \qquad (24)$$

Also, the population density of any vibro-rotational level can be calculated by multiplying $N(v_1 v_2^{\ell} v_3)$ by the rotational Boltzmann factor, i.e.

$$N(v_1 v_2^{\ell} v_3;J) = N(v_1 v_2^{\ell} v_3) \frac{g_J e^{-F_v(J)/k_BT_R}}{Q_R} \qquad (25)$$

where g_J is the statistical weight of the rotational level.

If the quantities T_R, T_2 and T_3 are known, the absolute population density of any vibro-rotational level is easily calculated from Eq. (25). We shall discuss the derivation of these temperatures from the gain measurements in the next section.

II-5 Vibrational and rotational temperatures in CO_2 laser

Despite the success of the mode temperature model in the modeling of CO_2 laser dynamics, experimental evidence to substantiate the theory has generally been indirect. Specifically, there has been no satisfactory and accurate method to measure directly the vibrational mode temperatures. The usual gain measurement carried out in the $00^0 1$ regular bands gave only the population difference between the upper ($00^0 1$) and the lower ($10^0 0$ or $02^0 0$)levels. Hence, no unambiguous information on the absolute population of the levels could be extracted.

Recently, the discovery of the sequence bands has provided a powerful tool to monitor the ν_3 mode vibrational temperature. Gain measurements on the sequence bands combined with measurements on the regular and hot bands enable us to determine accurately the absolute population of all the levels of interest. In the following, we shall outline the relationship between the gain and the vibrational and rotational temperatures in CO_2 lasers.

II-5.1 Sequence band transitions and asymmetric mode vibrational temperature

The use of sequence bands in the gain measurements enables a direct determination of the ν_3 model level populations. The method consists of measuring the gain ratio of the 00^02 sequence bands to the 00^01 regular bands. The gain ratio of any two lines in these bands can be written as:

$$\frac{\alpha_{00^02;J'_u}}{\alpha_{00^01;J_u}} = K(J'_u, J_u) \exp\left[-h\nu_3/k_BT_3\right] \qquad (25)$$

Where $K(J'_u, J_u)$ is a constant depending on the lines chosen. This constant is ~1.89, if the lines ($00^02 \longrightarrow 02^01$) P19 and ($00^01 \rightarrow 02^00$) P18 are used. Note that the gain ratio in Eq. (25) depends only on the vibrational temperature T_3. Once the temperature T_3 is determined from Eq. (25), the ν_3 mode vibrational energy, $E_3(T_3)$, can be calculated [62]. $E_3(T_3)$ is defined as the total vibrational energy stored in the ν_3 mode of CO_2 molecules and the vibrational mode of N_2 molecules, i.e.,

$$E_3(T_3) = N(X_{CO_2} + X_{N_2})h\nu_3\, x_3/(1-x_3) \qquad (26)$$

where N is the total number of molecules; X_{CO_2}, X_{N_2} are the fractional composition of CO_2 and N_2 in the gas mixture.

The ratio of $E_3(T_3)$ to the input energy is a direct measure of the pumping efficiency into the ν_3 mode of the laser system.

II-5.2 Hot band transitions and bending mode vibrational temperature

A knowledge of the lower laser level population is a key factor in modeling the temporal variation of the gain pulse (particularly the rise time of the gain [11]). The hot band transition ($01^11 \rightarrow 11^10$) has a maximum gain in the region of 11 μm. Based on the same principle as the measurement of the ν_3 mode temperature, the gain ratio of the hot band to the regular band is a measure of the bending mode temperature T_2. This can be seen by writing down the gain ratio between lines in the two bands, i.e.,

$$\frac{\alpha_{01^11;J'_u}}{\alpha_{00^01;J_u}} = K'(J'_u, J_u) \exp\left[-h\nu_2/k_B T_2\right] \qquad (27)$$

where the constant $K'(J'_u, J_u)$ depends on the lines chosen. This constant is 1.02, if the lines ($01^11 \rightarrow 11^10$) P(20) and ($00^01 \rightarrow 10^00$) P(18) are used. Hence T_2 can be determined directly from experimental measurements.

II-5.3 Rotational lines distribution and rotational temperature

Many relaxation rates in CO_2 gas mixtures depend very strongly on the gas temperature [57,64]. An increase of 200 K above room temperature can drastically reduce the efficiency of the TE pulsed lasers, and can terminate laser action in sealed-off CW lasers. Many methods have been developed to measure the gas temperature [63], but most of them are unsatisfactory for laser media due to insufficient temporal or spatial resolution, or because of excessive perturbation of the laser excitation region. An attractive and useful method for

determining gas temperature consists of measuring the rotational temperature via the rotational line distribution. A measurement of rotational temperature is equivalent to measuring the gas kinetic temperature, since the rotational relaxation rates are very fast ($\sim 10^{+7}$ sec^{-1} $torr^{-1}$), and equilibrium generally exists between the rotational distribution and the gas temperature.

The relationship between the gain coefficients and the rotational temperature can be obtained by writing down the ratio of gain between two vibro-rotational lines within a band. This ratio can be written as:

$$\frac{\alpha_{00^0 1;J'_u}}{\alpha_{00^0 1;J_u}} = K''(J_u, J'_u) \exp\left[-\frac{hc}{k_B T_R}\left(F_v(J'_u) - F_v(J_u)\right)\right] \qquad (28)$$

where $K''(J'_u, J_u)$ is a constant depending on the lines chosen, and F_v is the rotational energy. It can be seen that the ratio of gain depends only on the rotational temperature T_R. Therefore, by measuring the relative gain over many rotational lines within a band, we are able to determine the rotational temperature T_R by fitting the measured gain distribution to the calculated gain distribution.

II-6 Summary

This chapter has presented a brief review of CO_2 molecular structure and laser dynamics with emphasis on the calculation of the small-signal gain coefficient. A three temperature model (i.e. one rotational and two vibrational temperatures) for the gain calculation is described in detail, and will be used for comparison with experiment in Chapter V.

CHAPTER III

EXPERIMENTAL APPARATUS AND PRELIMINARY MEASUREMENTS

In this chapter, a detailed description is given of the apparatus used for making small-signal gain measurements in a TE CO_2 amplifier. The measurement of small-signal gain is a powerful method of investigating the characteristics of a laser system. The time dependence of the pulsed gain in TE CO_2 lasers is a measure of the relevant collisional relaxation rates, while the magnitude of the gain determines the population difference of laser levels. Furthermore, measurements of gain on several rotational lines and different vibrational bands enable the temperature of the discharge gas and of the vibrational modes to be determined. It is fortunate that gain measurements in TE lasers are relatively easy to make. Low pressure CW CO_2 lasers are ideal probes as they operate on the same transitions and wavelengths as the TE CO_2 laser. The CW laser used for these measurements will be described in detail, as will the TE pin-pin discharge system. The technique used to trigger the TE discharge, and the detection system are also described. Finally, some typical gain signals are presented.

III-1 Parallel pin-pin discharge amplifier

The first TEA CO_2 laser was developed by Beaulieu, who employed a linear pin-plane discharge system [1] . Subsequently, a number of techniques were used to obtain multiple transverse discharges distributed along a laser cavity [65]. For small volumes the resistive pin-pin system was very successful and found particular use in helical electrode arrangements for TEM_{oo} mode operation [66] . The development of double-discharge systems and E-beam pumped lasers [65] led to more efficient excitation of large discharge volumes. However, for the present study, the parallel pin-pin discharge is preferred for its simple construction and for its capability of working over a wide range of discharge mixtures and pressures. Furthermore, its spatial gain profile and gain uniformity along the length are known to be satisfactory [10].

The resistors used in any pin-pin discharge system must withstand repetitive, large current pulses for long periods of time. Reid [10] has found that Allen-Bradley carbon composite resistors give the best performance. The resistors, ½ watt 56Ω, were expoxied into 3.75 cm I.D. Perspex tubes, with a fixed anode-cathode spacing of 2.5 cm. The individual resistor spacing was 3.8 mm and the total discharge length can be varied from 23 cm to 92 cm.

The gas mixture to be excited flowed through the Perspex tube at ~1 l/min (N.T.P.). Coleman grade CO_2, high purity He and prepurified N_2 gases were used (as supplied by Matheson), and the flow rate of each gas was monitored by individually calibrated

flowmeters. The flowmeter calibrations were accurate to better than 2%. The gases were mixed by a series of baffles before they entered the discharge volume, and were pumped out by a oil-free Busch 010-112 Super rotary vacuum pump. This pump maintained an adequate gas flow at pressures from 10 torr to one atmosphere. The ends of the discharge tube were sealed by O-ring mounted NaCl Brewster windows. Vacuum fittings were used throughout the gas-handling system. Care was taken to minimize leaks into the discharge volume, resulting in a total leakage rate of less than 4 torr/l-hr.

The gas mixtures were excited by discharging a low inductance capacitor through the resistor array. The circuit used is typical of the simple circuits employed in high-voltage pulsed lasers [66], it is shown schematically in Fig. 6. The power supply (Universal Voltronics) is capable of delivering 25 mA current at a maximum voltage of 32 kV. The spark-gap (EG & G, GP 14-B, oil immersed) was fired by a high-voltage trigger module (EG and G TM 11) which is triggered in turn by a pulse generator (Data-Pulse 100A). The storage capacitors used in the experiments were all rated to 50 kV, and ranged in value from 1 nF to 20 nF. All connections were kept as short as possible, and four thick copper braids were used to improve the energy distribution along the discharge length and also to reduce the inductance of the discharge circuit.

This simple discharge circuit was found to give very stable operation without any arcing over wide range of gas mixture and pressure, for all the discharge energies used in this work.

FIGURE 6

Schematic diagram of the discharge circuit. Also shown are typical current and voltage pulses obtained when a 20 nF capacitor, charged to 20 kV, was discharged through a 3% CO_2: 97% He mixture at atmospheric pressure.

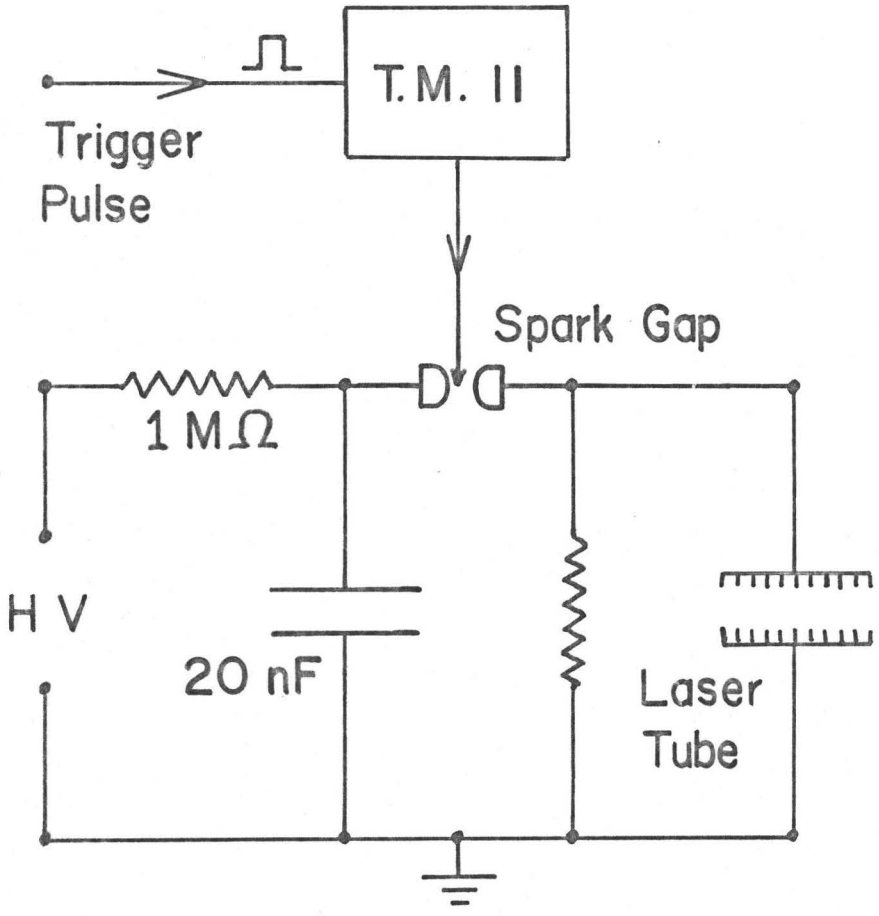

DISCHARGE CIRCUIT

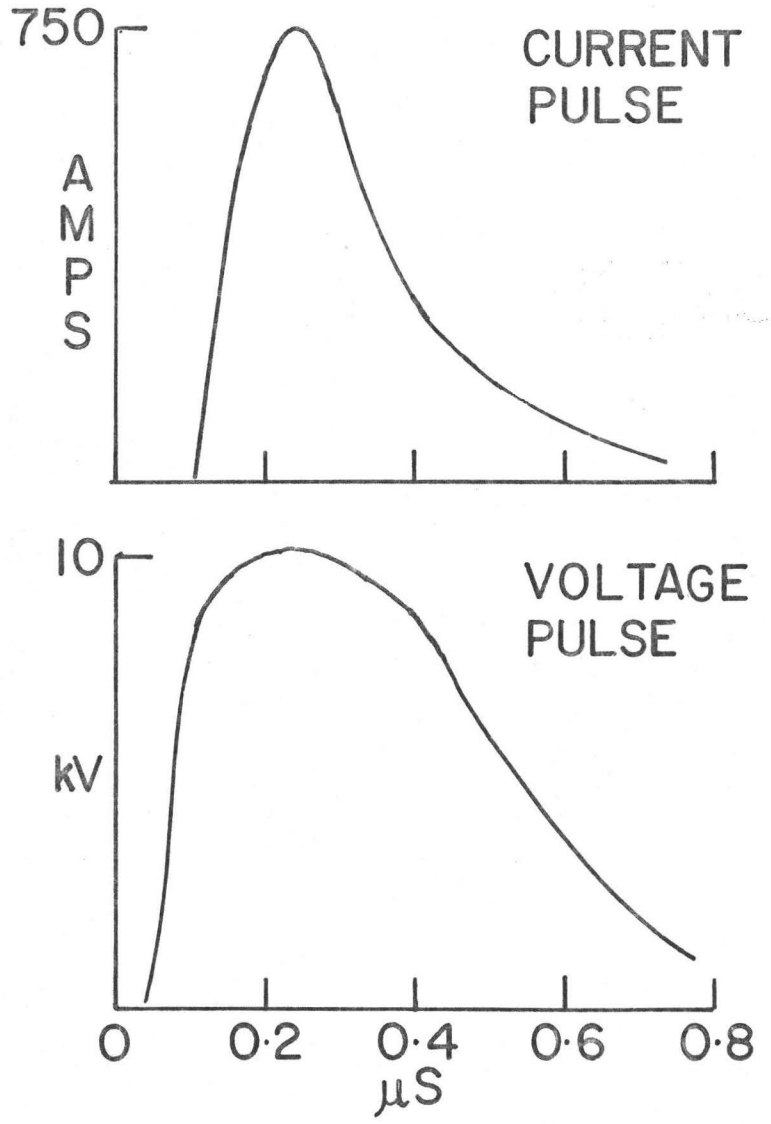

III-2 Gain measurement set-up

The technique described here for measuring small signal gain in a TE discharge is the same as that used by Jacobs [67] and by Reid [10]. Fig. 7 is a schematic diagram of the entire apparatus; the individual components are described in detail below.

(a) CO_2 Probe laser

A stable, low pressure CW CO_2 laser was constructed for these measurements. A sealed-off gain tube of 55 cm discharge length containing a mixture of 10% CO_2:20% N_2:70%H_e at ~10 torr total pressure was excited by a stabilized dc power supply. The laser tube could be easily refilled through a high vacuum valve. Currents of 7 to 10 mA were used, and the laser was cooled by circulating methanol at ~-3°C. The gain tube was mounted in a cavity consisting of a grating and a 3 m radius mirror separated by Invar rods. The grating and mirror supports were also made of Invar to ensure good thermal stability. The grating was a gold-coated replica (PTR Optics ML-303), blazed at 10.6 μ, and laser ouput was obtained through the 2% transmitting mirror. This mirror was mounted on a sensitive micrometer drive for fine tuning of the total cavity length. A cell of 25 cm length was inserted in the laser cavity. The gas in this cell could be heated to ~400°C by means of an internal heater coil. This convenient set-up enabled us to obtain laser action on the regular and sequence bands by simply evacuating the hot cell or by filling it with 50 torr of pure CO_2. To switch from regular band to sequence band took only 15 minutes.

FIGURE 7

Schematic diagram of the apparatus used for measuring small-signal gain.

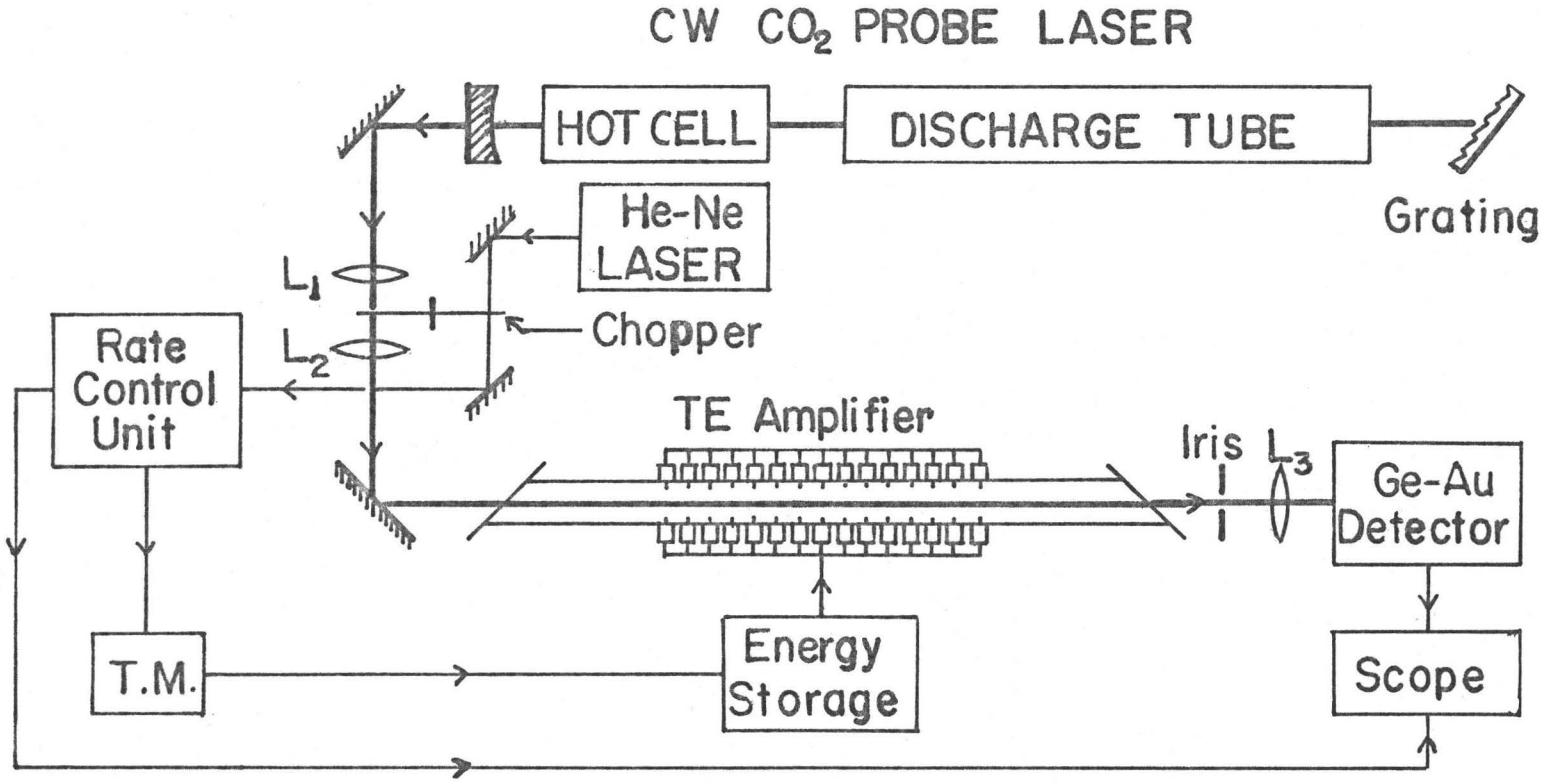
CW CO_2 PROBE LASER
HOT CELL
DISCHARGE TUBE
Grating
He-Ne LASER
L_1
L_2
Chopper
Rate Control Unit
TE Amplifier
Iris
L_3
Ge-Au Detector
T.M.
Energy Storage
Scope

The laser operated in the fundamental TEM_{00} mode with an output power of approximately two watts for the regular bands and half a watt for the sequence bands. The internal grating allowed the output to be tuned over many lines in the P and R branches of both the regular and sequence bands. Amplitude stability was better than 2% in the short term, but thermal effects caused the cavity length to drift from line center over a period of hours. This was easily corrected by manually retuning the output mirror, on operation which took only a few seconds. This CW laser proved to be an ideal probe for the measurement of gain in TE amplifiers. However, with this short gain tube, laser action on the hot band could not be achieved, and a longer gain tube was constructed for the hot band measurements described in Chapter V.

(b) Chopper system

It is convenient to use a chopped probe beam, as opposed to a continuous beam, for this type of gain measurement. This enables ac detection methods to be employed, and the beam amplitude can easily be continuously monitored. By chopping with a low duty-cycle, the detector can be protected from overheating. The lenses used in the chopper system also served to focus the probe beam into the TE amplifier. The probe beam passed through two 1" focal length Ge lenses, L_1 and L_2, (Oriel A-11-741-11) spaced approximately 2" apart. The beam was chopped by a spinning disc at the common focus of the two lenses. This arrangement produces fast rise and fall-times in the probe pulse.

One of the lenses was mounted on a micrometer driven X-Y-Z positioner. Adjustments in the X and Y direction enabled the probe beam to be deflected horizontally and vertically, and by carefully adjusting the separation of the lenses, the probe beam could be focussed at the centre of the TE amplifier. The effective beam diameter in the discharge was kept as small as possible, and the spot diameter was generally less than 3 mm (1/e intensity) throughout the discharge region. This ensured that reasonably accurate measurements of spatial gain distributions could be made. A beam pulse repetition rate of approximately 100 p.p.s. was used. This was ideal for monitoring the amplitude of the probe beam, but was much too fast to serve as a trigger for the TE amplifier discharge.

The method used to trigger the amplifier discharge circuit is similar to that employed by Jacobs [67], modified to permit electronic control of the repetition rate of the amplifier. The rotating chopper wheel periodically admitted the CW probe beam and a 6328 $\mathring{A}$ He-Ne laser "trigger" beam through two separate small slots located 180^{o} apart. The "trigger" beam fell upon a photodiode and the resulting train of pulses was fed to a repetition rate control unit. This reduced the pulse repetition rate to 2 or 3 p.p.s. while maintaining the time synchronisation. Figure 8 shows a typical gain signal superimposed upon the modulated probe laser signal. Note that this scheme yields a single oscilloscope trace of the probe beam amplitude prior to, during, and after amplification. The time-delay to the amplifier could be adjusted to locate the gain pulse anywhere

FIGURE 8

Typical gain signal for the ($00^{o}1$) regular bands (a and c) and the ($00^{o}2$)sequence bands (b and d). Gas mixture is 13% CO_2:10% N_2:77% He at 92 torr, and amplifier length is 92 cm. Time scales are: 200 μsec/div for a and b, and 20 μsec/div for c and d.

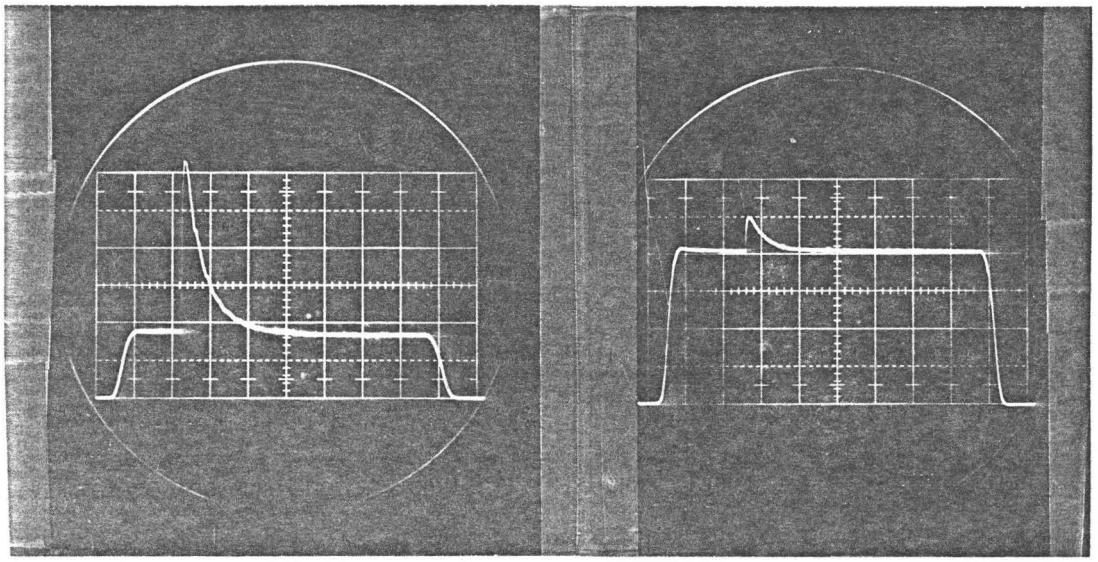

(a) (b)

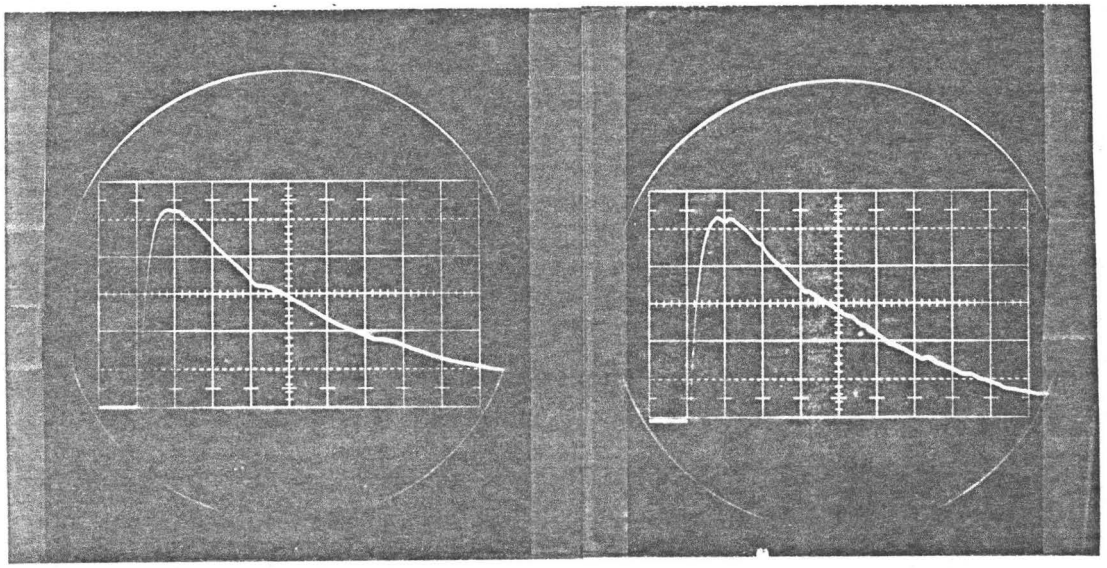

(c) (d)

on the probe signal. This enabled the time base to be expanded to determine risetimes, or compressed to examine the absorption after the amplifier pulse. Further advantages of this technique are described by Jacobs [67].

(c) Detection system

A Ge:Au detector (SBRC-40742) cooled with liquid nitrogen, was used in the gain measurements. This is a photo-conductive device with a risetime of 2 ns into a 50 Ω load. However, in order to increase the sensitivity of the detector, the load resistor was varied from 1 to 5 kΩ. The detector signal was amplified by a Tektronix 1A7A Plug-in unit (bandwidth 1 MHz) and displayed on a Type 556 dual-beam oscilloscope. The risetime of the entire detection system was ∿300 ns. This is fast enough for all the required measurements. After passing through the TE amplifier, the probe beam was directed onto the detector element by a 1" focal length Ge lens, L_3 (Oriel A-11-741-11). A 90 volt bias was used in the detector circuit, and the resultant signals were ∿100 mV with less than 1.0 mV background noise.

III-3 Preliminary measurements

It is worthwhile, at this stage, to mention some problems encounted in the measurements and to discuss briefly the main features observed in the temporal behavior of gain signal.

III-3.1 Small-signal gain measurement

Before any accurate gain measurements were made, several checks were carried out to ensure that the signal obtained from the

detector truly represented the gain in the TE amplifier. With the probe beam switched off, the amplifier was fired and a check made to ensure that the noise coming from the discharge was small, and that the spontaneous radiation reaching the detector was not significant. Then, the probe beam was passed through the amplifier, and a series of measurements was made to ensure that the gain measured under all conditions remained constant when the probe signal was attenuated by a factor of 2, confirming that the gain was measure in the small-signal gain region. Finally, a series of measurements on the detector system ensured that its response was linear over the anticipated range of intensities. The entire apparatus was operated for a period of several months with no significant problems. With the TE amplifier operating in a region of good stability, the total gain in the amplifier of 92 cm length could be measured to an accuracy of 5% or better for values above .3, and of 10% for values below this level. These measurements were reproducible from pulse-to-pulse and day-to-day. With this good stability and high accuracy, the measurements on the weak sequence gain could be performed with ease.

III-3.2 Temporal behavior of the gain signal

Typical gain signals are displayed in Figure 8 and some important features will be discussed. In Figs. 8a and 8b, the gain signal is superimposed on the probe signal (i.e. square pulse), two features are observed: firstly, the gain of sequence line is much smaller than that of regular line for this low input energy ($\sim$100

J/l-atm); secondly, a small absorption is observed at the tail of regular gain pulse (Fig. 8a), but none for the sequence gain pulse (Fig. 8b). This holds true for all input energies. The absorption at the tail of regular gain pulse becomes more and more apparent at high input energies (see Appendix B).

Expanded gain signals are shown in Figs. 8c and 8d. Two features are observed: firstly, the fall time of the regular gain signal is $\sim$ twice as long as that of the sequence gain signal (as expected from harmonic oscillator approximation); secondly, small periodic ripples are present in both gain signals (noise fluctuations are also present on Fig. 8d). These ripples are due to the shock wave produced in the discharge volume. The time between ripples is $\sim$65 μsec, corresponding to the time taken for the shock wave to cross the amplifier tube. The magnitude of the ripples was minimized by careful alignment of lens L_3; they did not significantly interfere with measurements of gain peaks, but limited the accuracy of measurements of fall time at high input energies. The discharge plasma caused no other detectable changes in the probe beam, e.g., lensing effects in the amplifier were negligible [66].

III-4 Summary

This chapter given a detailed description of the experimental apparatus used for the present study. Some important features of the gain signal of both the regular and sequence bands are discussed. The next two chapters deal with the variation of the magnitude of gain as a function of input energy and gas mixture.

CHAPTER IV

GAIN LIMITATIONS IN TE CO_2 LASER AMPLIFIERS

In this chapter, the factors which limit the small-signal gain in TE CO_2 laser amplifiers are experimentally investigated, and the physical processes responsible for the reduction of gain at high input energy are discussed. One major result of the present study is the discovery that the ν_3 mode vibrational temperature, i.e. T_3, saturates at high input energy. It is this saturation which sets a basic limit to the attainable gain in TE CO_2 laser amplifiers. Finally, the effects of N_2 and CO_2 in the CO_2-N_2-He laser mixture are examined, and some important features emerging from this study are discussed.

IV-1 Gain characteristics

The magnitude of the small-signal gain in a typical TE CO_2 discharge depends upon the input discharge energy and the gas mixture. However, it is found that, for all mixtures the gain initially increases rapidly with input energy, then levels off and begins to fall as the input energy is increased beyond a certain level of pumping. Figure 9 shows clearly that the reduction of the gain at high input energy occurs for both the regular line 9.4 μm $00^0 1$ P(18), and the sequence line 9.3 μm $00^0 2$ P(19) in a 13% CO_2:10% N_2:77% He mixture. Similar behavior has been observed for all lines of regular bands, for all gas mixtures and for all pumping systems [5,6,8]. Note that the gain does

FIGURE 9

Variation of gain with input energy for two typical lines of the regular and sequence bands in a 13% CO_2:10% N_2:77% He mixture. Several storage capacitors were used; data points taken with a 1 nF capacitance are represented by □, while O, Δ and ● represent 5, 10 and 20 nF respectively. For each capacitance, different discharge lengths (varied from 23 to 92 cm) and different applied votages (varied from 18 to 26 kV) were used.

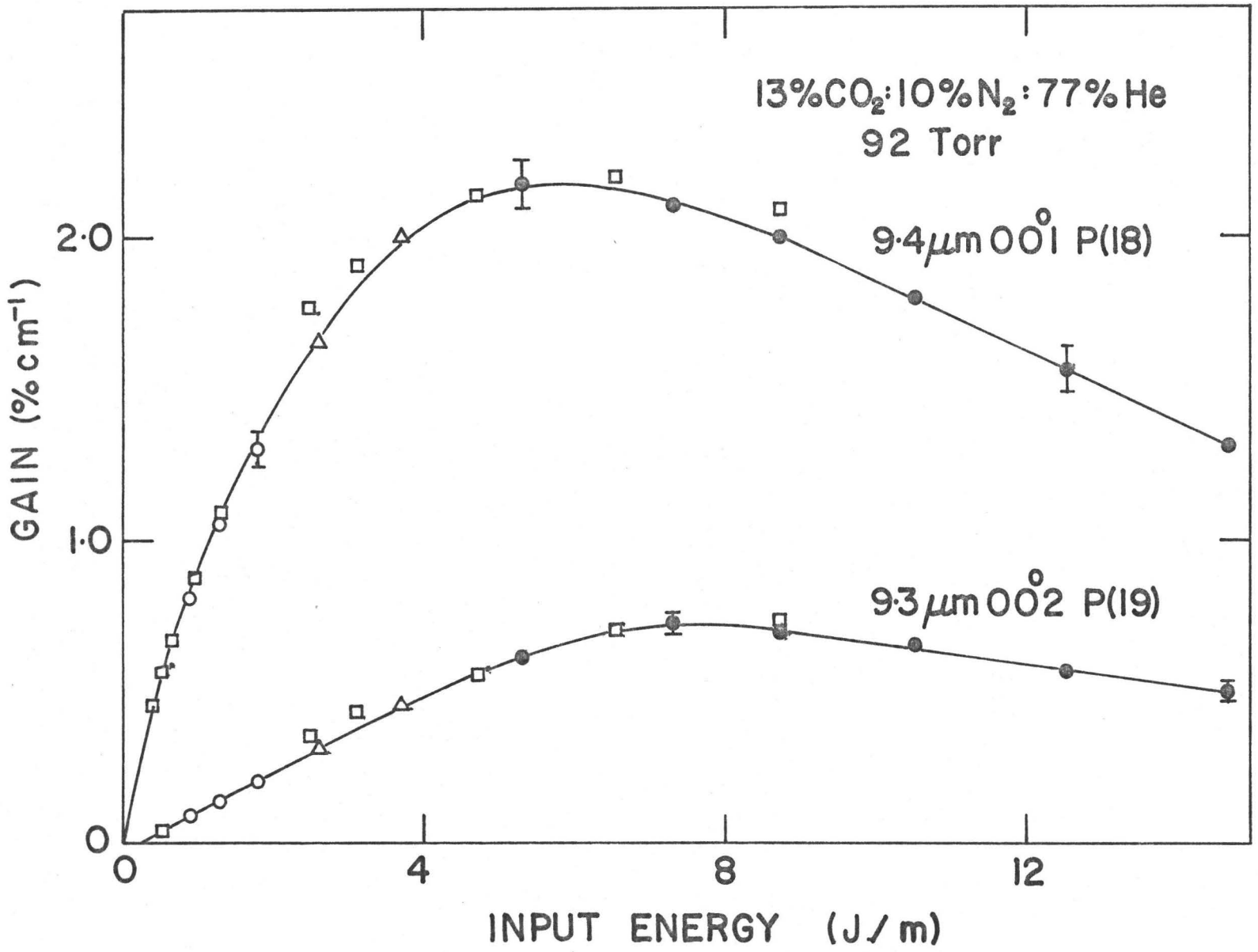
13%CO2:10%N2:77%He
92 Torr
9·4μm 00°1 P(18)
9·3μm 00°2 P(19)
GAIN (%cm⁻¹)
2·0
1·0
0
0
4
8
12
INPUT ENERGY (J/m)

not depend upon the actual discharge length, applied voltage or storage capacitor, provided the ratio of stored energy to the discharge length remains constant. It should be pointed out that in the present experiment, the input energy to the gas is denoted simply by the ratio of the capacitor storage energy to the discharge length (i.e. the unit is Joule/meter). While this unit is convenient for the present study, it is difficult to compare our results with other work, because the common unit employed for the input energy is Joule/liter-atm. The conversion factor between these two units, i.e. J/m to J/l-atm, is derived in Appendix A. The two units will both be displayed on the abscissa scale where appropriate.

In the present study, the 9.4 μm CO_2 laser bands are used, because the ratio of the vibrational matrix element of the $00^0 2$ level to that of the $00^0 1$ level is known only for the 9.4 μm band [46]. The two rotational lines, $00^0 2$ P(19) and $00^0 1$ P(18), are chosen to be representative of the CO_2 laser bands, because these two lines have the highest gain in their respective bands, and have no accidental overlapping with other rotational lines. Furthermore, the gain ratio between these two lines is insensitive to changes in the rotational temperature [68] and therefore provides an accurate determination of the ν_3 mode vibrational temperature.

The reduction of gain at high input energy (as shown in Fig. 9) has generally been believed to be due to thermal effects such as increase of gas temperature and discharge deterioration. However,

Ballik et al. have considered these two effects in their work [10], and concluded that they are not sufficient to account for the observed gain reduction. In the present study, a new method based on gain measurements of both the sequence and regular bands allows us to separate discharge excitation to the ν_3 mode from thermal effects, hence enabling us to measure the saturation in the discharge excitation of the ν_3 mode.

IV-2 ν_3 mode vibrational temperature

(a) Saturation of ν_3 mode vibrational temperature

As outlined in Section II-5.1, the ratio of gain of the sequence bands to the regular bands allows us to determine the ν_3 mode temperature, i.e. T_3, which in turn allows us to calculate the ν_3 mode vibrational energy $E_3(T_3)$. The ν_3 mode levels are the upper levels of the laser transitions, and since the lower laser levels relax much faster than the upper laser levels (this will be shown in Section V-1. See also Ref. 11), the degree of excitation of the ν_3 mode is a crucial factor in the performance of the CO_2 laser. More precisely, the increase of the ν_3 mode vibrational energy versus the input energy indicates the net pumping efficiency into the ν_3 mode. Figure 10 shows a plot of T_3 versus input energy for a 13% CO_2:10%N_2:77%He mixture where T_3 is the ν_3 mode vibrational temperature at the gain peak. It can be clearly seen from Fig. 10 that the ν_3-mode temperature saturates at high input energy. Since the population of the upper laser levels ceases to increase at high input energy, any further increase of input energy only heats the gas mixture, and populates the lower laser levels.

FIGURE 10

Variation of ν_3 mode vibrational temperature with input energy in a 13% CO:10% N_2:77% He mixture. Results are obtained from the ratio of gain coefficients shown in Fig. 9.

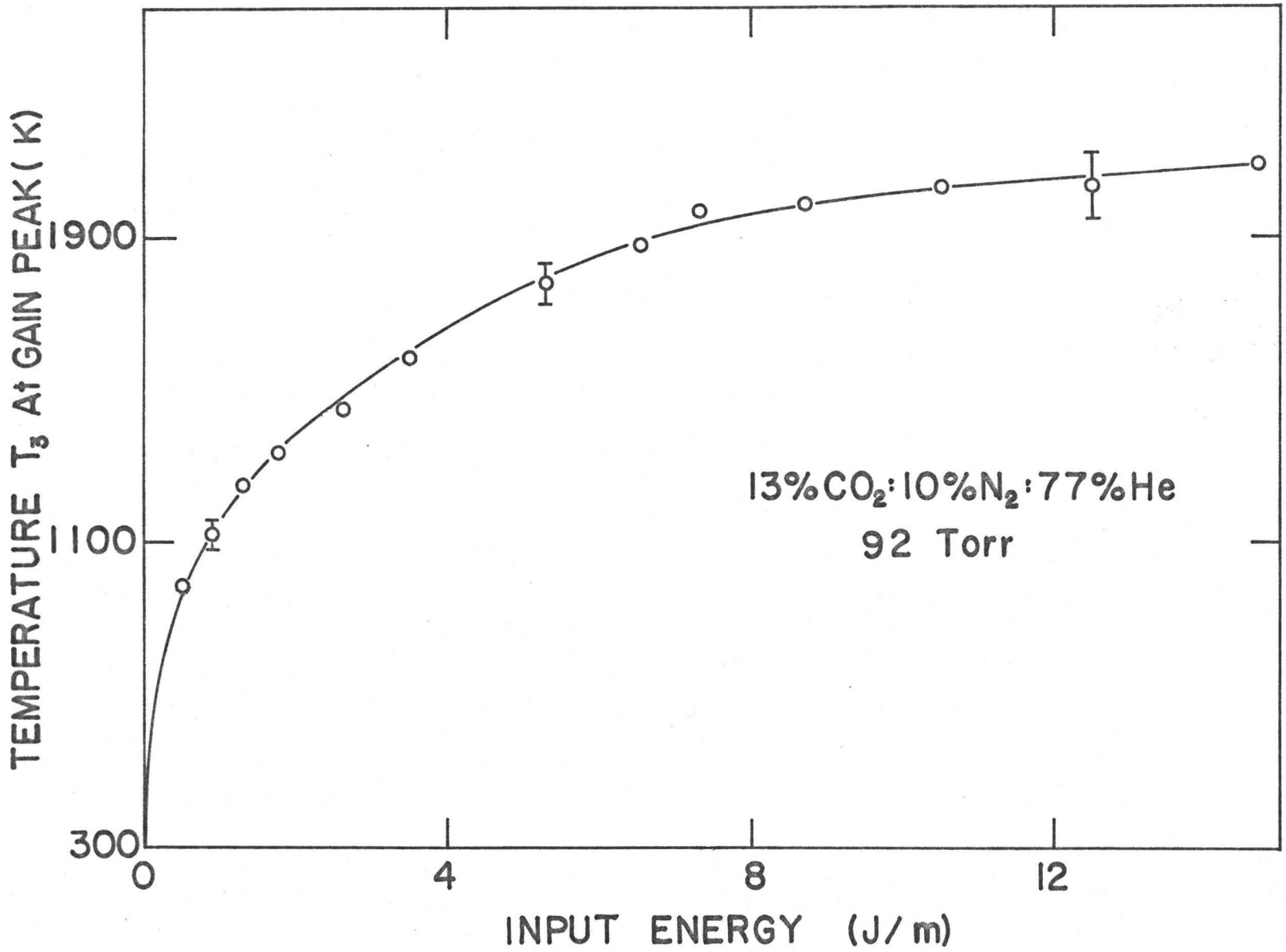
TEMPERATURE T_3 At GAIN PEAK (K)
1900
1100
300
0
4
8
12
INPUT ENERGY (J/m)
13%CO_2:10%N_2:77%He
92 Torr

Hence, the gain falls at high input energy. However, before any definitive conclusions can be drawn about the pumping efficiency to ν_3 mode, we must account for the ν_3 mode relaxation processes which occur in the time interval between the end of the current pulse and the peak of the gain pulse. It is the total ν_3 mode vibrational energy at the end of the current pulse which is a fundamental quantity of the discharge dynamics.

(b) Reduction of pumping efficiency to ν_3 mode

To calculate the ν_3 mode vibrational energy immediately after the current pulse, the population of the 00^01 and 00^02 levels is extrapolated back to the time t = 0 using the decay of the gain pulse. Figure 11 shows a plot of gain versus time on a semilog scale as derived from oscilloscope photographs of the gain pulse. The resulting straight lines are consistent with an exponential decay of the levels [69]. It should be noted that after the gain peak, the decay of the gain pulse is due to the relaxation of the populations of the upper laser levels. During this time, the populations of the lower laser levels are in near equilibrium with the gas temperature (see Section V-1) and are negligible compared to that of the upper laser levels (except at the end of the gain pulse). By extrapolating the gain pulse back to time t=0, the initial populations of the (00^02) and (00^01) levels are obtained, and the initial ν_3 mode vibrational energy is derived from these initial populations. An important remark should be made. Immediately after the discharge, the ν_3 mode CO_2 molecules may assume a vibrational mode temperature different from that of the N_2 molecules.

FIGURE 11

Typical decay of gain signals with time for the regular and sequence bands. Results are obtained from photographs c & d in Fig. 8. The inverse of slope of the straight lines represents the decay time of the level. The decay time of the ($00^{0}1$) level is $\sim$ twice as long as that of the ($00^{0}2$) level (as expected from harmonic oscillator approximation).

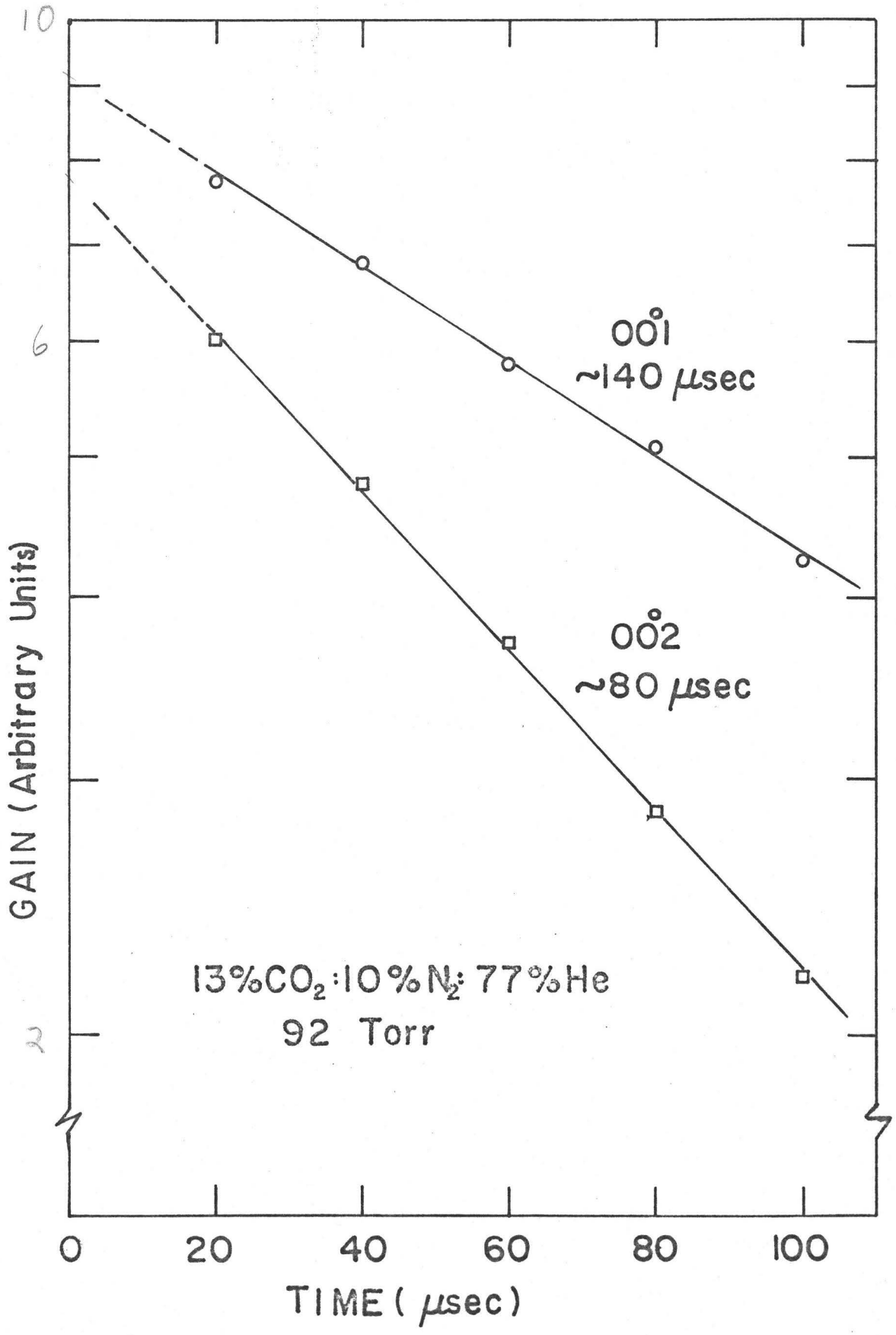
10
6
2
GAIN (Arbitrary Units)
00°1
~140 μsec
00°2
~80 μsec
13%CO2:10%N2:77%He
92 Torr
0
20
40
60
80
100
TIME (μsec)

Subsequently, V-V energy exchange brings the two resonant modes into equilibrium at the same vibrational temperature prior to the gain peak. Therefore, the initial ν_3 mode vibrational temperature calculated from the extrapolated values of population at t = 0 represents an equilibrium value of T_3 and gives us an accurate measurements of the total ν_3 mode vibrational energy stored in the CO_2 and N_2 at t = 0.

Figure 12 shows a plot of $x_3/(1-x_3)$(which is proportional to the total ν_3 mode vibrational energy) at t = 0, versus the input energy for a 13% CO_2:10%N_2:77%He mixture. In the same Figure, the value of $x_3/(1 - x_3)$ at gain peak ($t \sim 20$ μsec) is also plotted for the same mixture. It can be seen that the correction obtained by extrapolating back to t = 0 is only significant at high energies where the molecular relaxations of the ν_3 mode have become relatively fast [57]. Even for the most extreme case, the correction is only ~20%. As the pumping efficiency to the ν_3 mode is proportional to the ratio of $x_3/(1 - x_3)$ to input energy, it is very clear from Fig. 12 that the pumping efficiency to the ν_3 mode <u>decreases</u> with increasing input energy. As our measurement technique is direct, and accounts for both thermal effects and molecular relaxations, one must conclude that there exists some mechanism in the CO_2 discharge which limits the pumping efficiency to the ν_3 mode at high input energies. To determine more about this mechanism, we have investigated the variation of the saturation of the ν_3 mode energy with gas mixture.

FIGURE 12

Variation of $x_3/(1-x_3)$ with input energy for a 13% CO_2:10% N_2:77% He mixture. The dashed line indicates the pumping efficiency to the ν_3 mode at low input energy. □ , O are experimental points.

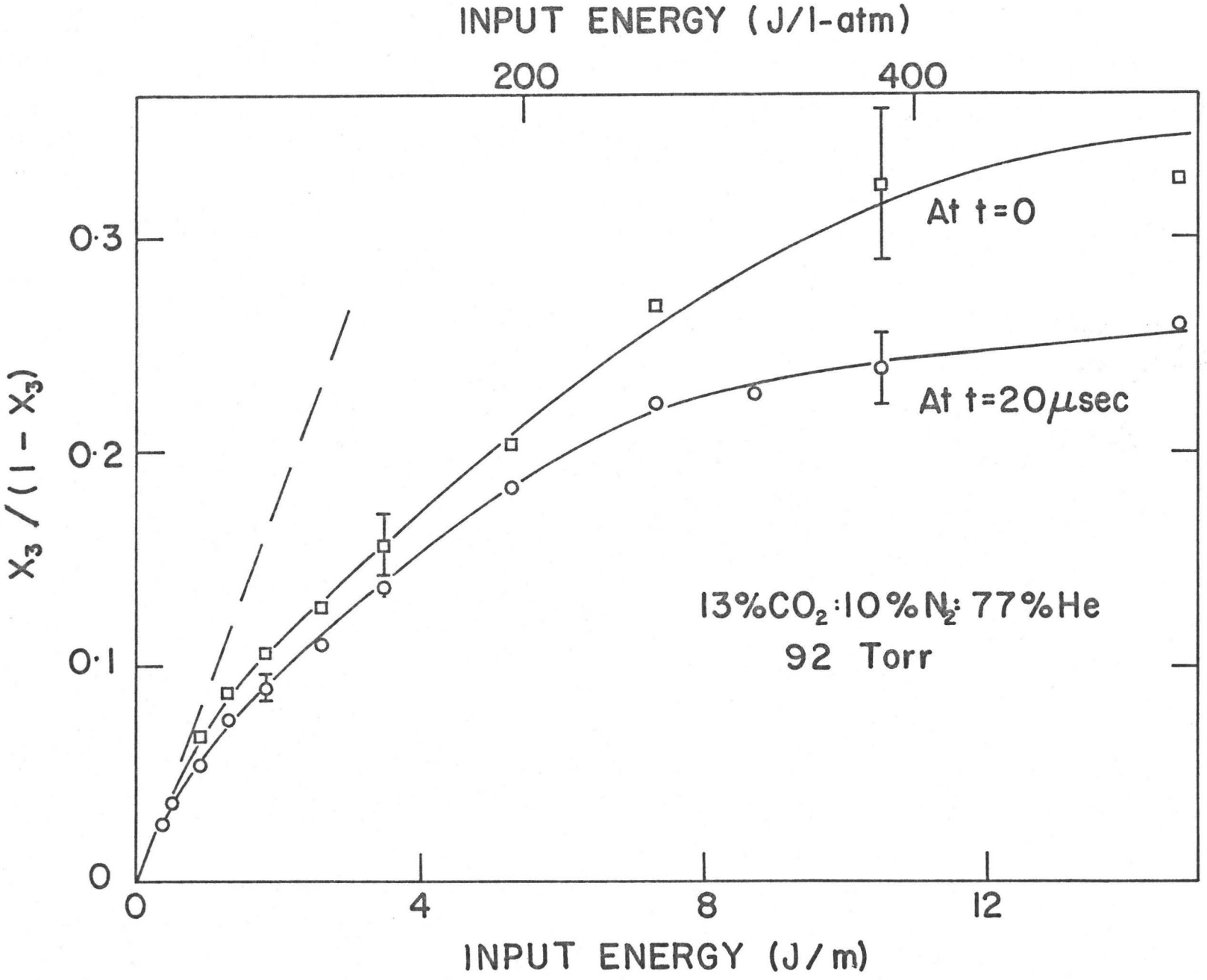
INPUT ENERGY (J/l-atm)
200
400
0·3
0·2
0·1
0
$X_3 / (1 - X_3)$
At t=0
At t=20μsec
13%CO₂:10%N₂:77%He
92 Torr
0
4
8
12
INPUT ENERGY (J/m)

(c) Variation with mixture

The above results were obtained for the 13% CO_2: 10% N_2:77% He mixture which is typical of those used in CO_2 lasers. However, it is important to consider separately the effect of CO_2 and N_2 on the saturation behavior. Two extreme cases are therefore examined: the one is a 3% CO_2:97% He mixture with no N_2; the other is a 3% CO_2:21% N_2: 76% He mixture with high N_2 to CO_2 ratio (In a N_2-He mixture alone, i.e. no CO_2, there is no gain, and hence a small trace of CO_2 is added to the N_2-He mixture to enable us to monitor the vibrational energy in the discharge). The results obtained for these two mixtures are shown in Figs. 13 and 14 which are plots of $x_3/(1 - x_3)$ versus input energy at t = 0, and at gain peak respectively. Once again, we notice that the pumping efficiency decreases substantially at high input energies for both mixtures. The main difference between the two mixtures is in the magnitude of energy stored in the ν_3 mode. For the 3% CO_2:21% N_2:76% He mixture, a vibrational temperature as high as $\sim 3000^{o}K$ is attained, which is much higher than $\sim 1800^{o}K$ observed for the 3% CO_2:97% He mixture at the same input energy.

The pumping efficiencies to the ν_3 mode for these mixtures are summarized in Table III, together with the theoretical predictions at low input energy. For the 3% CO_2:21% N_2:76% He mixture, the pumping efficiency to the ν_3 mode is $\sim$84% at low excitation energy, this is in good agreement with the work of Lowke et al. [70] which predicts a pumping efficiency of $\sim$78%. The agreement with theory is generally satisfactory in spite of some uncertainties in the amount of energy discharged into the gas and the energy distribution within the discharge volume.

FIGURE 13

Variation of $x_3(1-x_3)$ with input energy for a 3% CO_2:97% He mixture. The dashed line indicates the pumping efficiency to the ν_3 mode at low input energy. ◘ , O are experimental points.

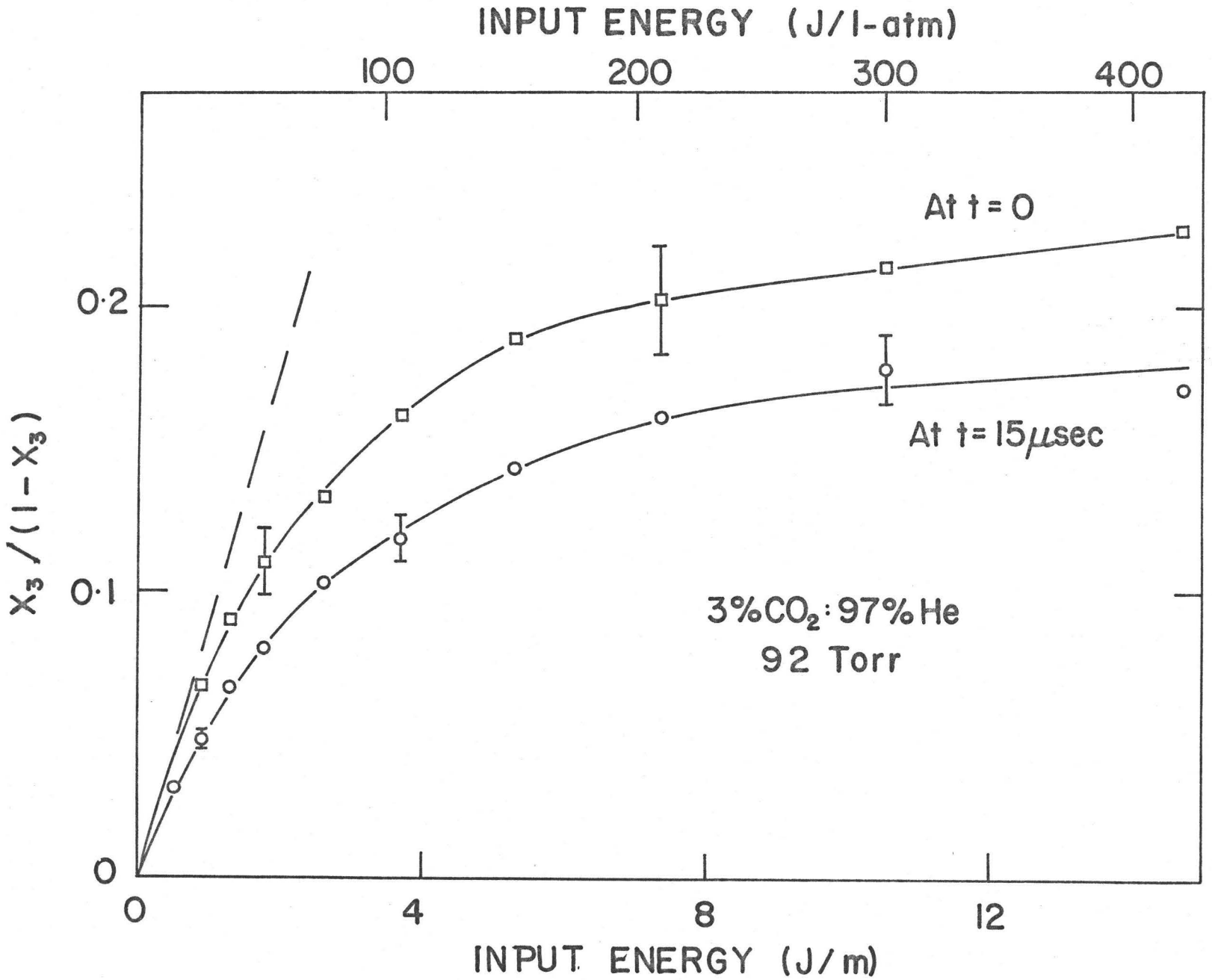
INPUT ENERGY (J/l-atm)
100
200
300
400
At t = 0
At t = 15μsec
0·2
0·1
0
$X_3/(1-X_3)$
3%CO_2:97%He
92 Torr
0
4
8
12
INPUT ENERGY (J/m)

FIGURE 14

Variation of $x_3(1-x_3)$ with input energy for a 3% CO_2:21% N_2:76% He mixture. The dashed line indicates the pumping efficiency to the ν_3 mode at low input energy. □ , O are experimental points.

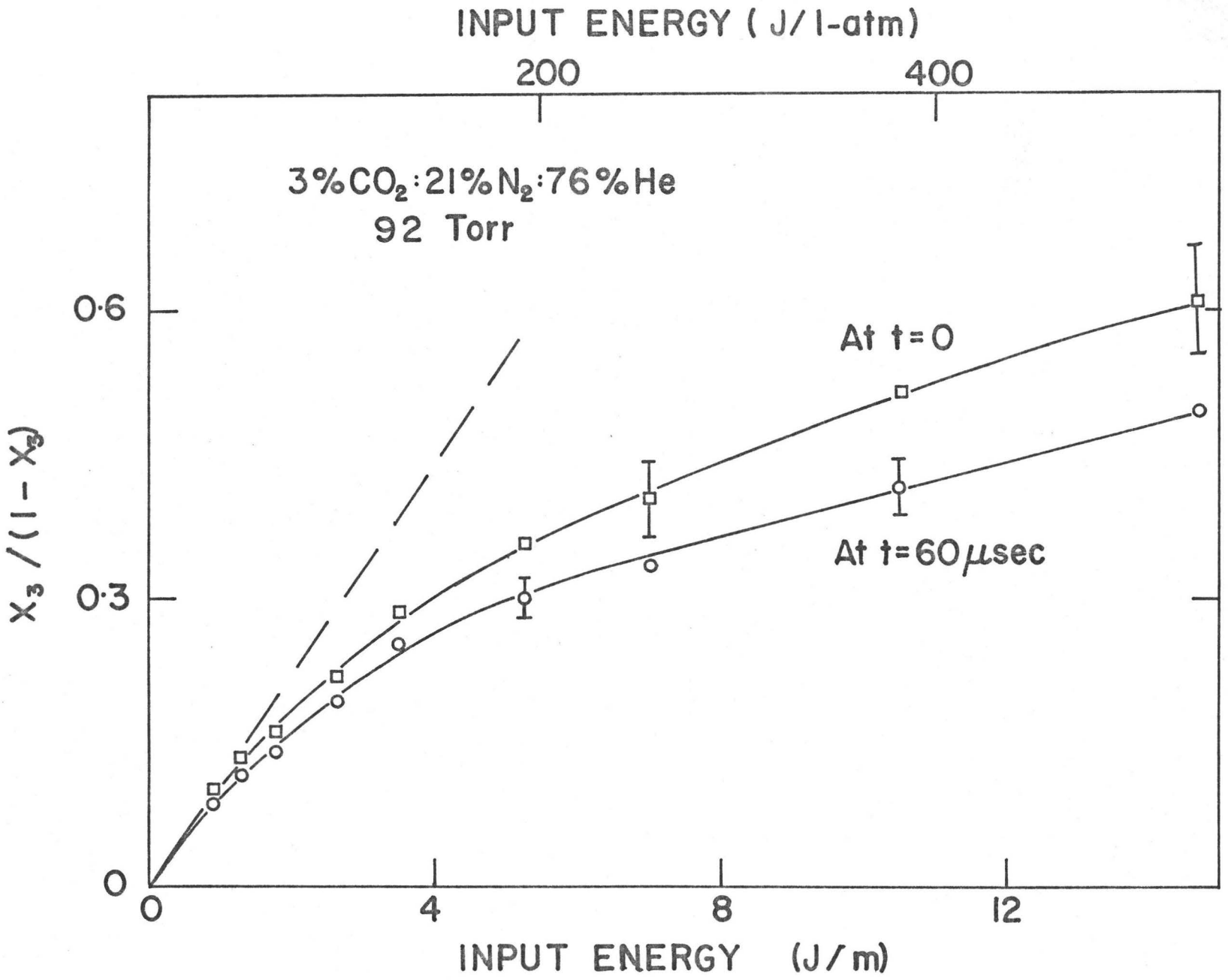
INPUT ENERGY (J/ l-atm)
200
400
3%CO2:21%N2:76%He
92 Torr
At t=0
At t=60μsec
0·6
0·3
0
X3 /(1 – X3)
0
4
8
12
INPUT ENERGY (J/m)

TABLE III

PUMPING EFFICIENCY TO THE ν_3 MODE, $\varepsilon(\nu_3)$, FROM EQ. (A-2)

	Experimental $\varepsilon(\nu_3)$ at input energy (J/l-atm)				Theoretical prediction
Mixture CO_2:N_2:He	~ 0	100	200	400	
3%: 0 :97%	11%	5.7%	3.7%	2.0%	5% (a)
13%:10%:77%	64%	36%	29%	22%	53% (b)
3%:21%:76%	84%	67%	51%	36%	78% (b)

(a) Ballik et al. [10]

(b) Lowke et al. [70]

However, the theory is unable to predict the reduction of pumping efficiency at high input energy [11]. From Table III, it can be seen that the pumping efficiency for the 3% CO_2:97% He mixture is reduced by a factor of 5.5 at ~400 J/ℓ-atm from that at low input energy. This reduction factor is only ~2.5 for the 3% CO_2:21% N_2:76% He mixture. The presence of N_2 obviously has a beneficial effect on the CO_2 laser operation.

To determine further the characteristics of CO_2 and N_2 in a self-sustained glow discharge, a series of measurements were made at a fixed input energy ~500 J/l-atm for very different mixtures where the helium content is held constant (For a constant He content, the value of E_G/N, i.e. the ratio of quasi-stable electric field between electrodes to the number density of molecules, for a pulsed self-sustained glow discharge, is approximately constant [13]). A high input energy is used in this study to ensure that the total ν_3 mode vibrational energy is close to saturation. We were therefore able to determine how the saturation energy depends upon gas mixture. The total ν_3 mode vibrational energy, $E_3(T_3)$, is proportional to the quantity $(X_{CO_2} + X_{N_2})\, x_3/(1 - x_3)$ at t = 0 which is found to decrease linearly with the mixture ratio $X_{CO_2}/(X_{CO_2}+X_{N_2})$ for a fixed He content. Figure 15 shows a plot of $(X_{CO_2} + X_{N_2})\, x_3/(1 - x_3)$ versus $X_{CO_2}/(X_{CO_2} + X_{N_2})$ where X_{CO_2}, X_{N_2}, X_{He} are respectively the fractional composition of CO_2, N_2 and He in the mixture. Several important conclusions can be reached. The ν_3 mode vibrational energy which can be stored in a N_2-He mixture is <u>much more</u> than that of a CO_2-He mixture.

FIGURE 15

Variation of the quantity $(X_{CO_2} + X_{N_2})\, x_3/(1-x_3)$ with the mixture ratio $X_{CO_2}/(X_{CO_2} + X_{N_2})$ for two fixed He contents (see text). □, O are experimental points. Solid lines are the best fit lines.

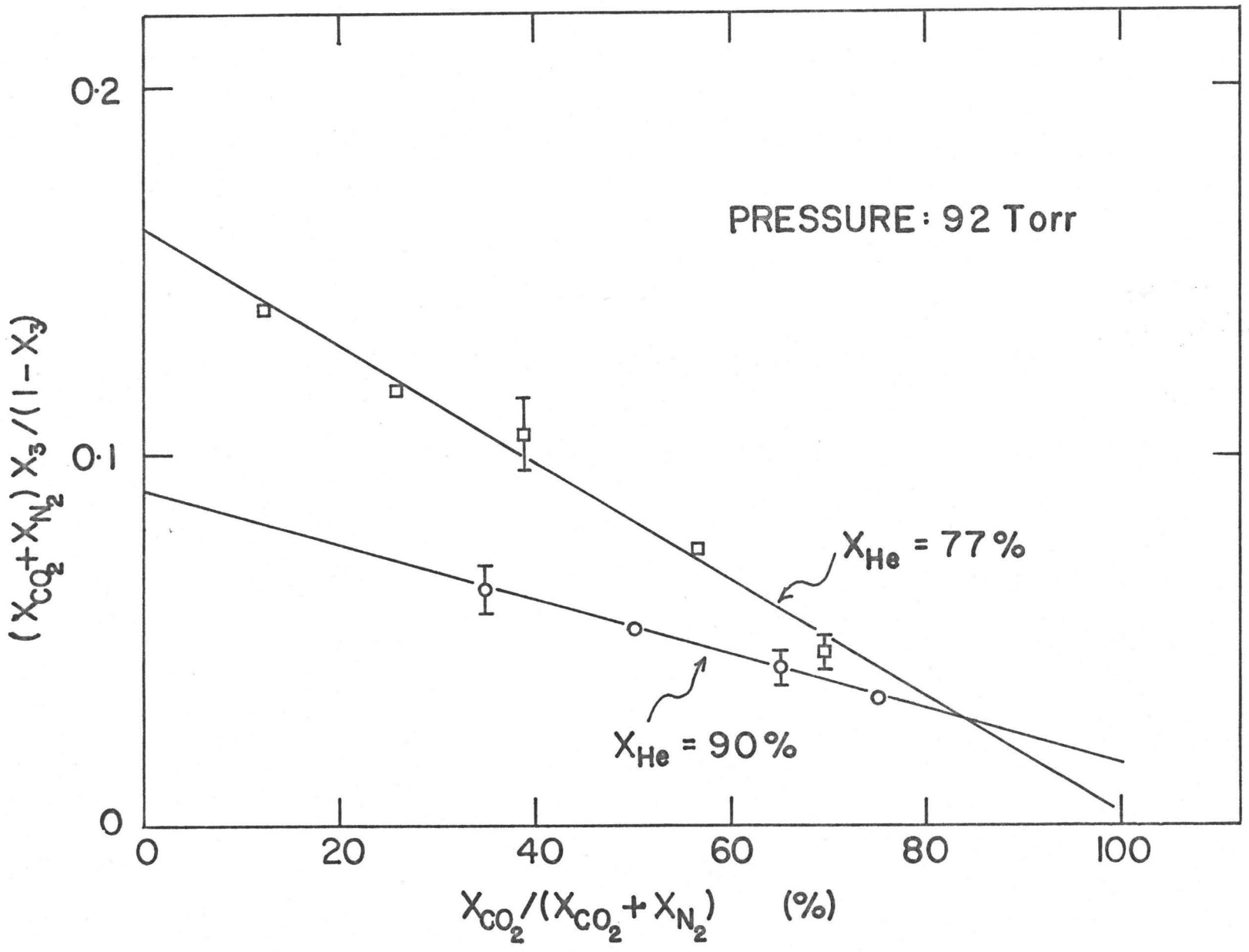
PRESSURE: 92 Torr
X_{He} = 77%
X_{He} = 90%
$(X_{CO_2}+X_{N_2})\,X_3/(1-X_3)$
$X_{CO_2}/(X_{CO_2}+X_{N_2})$ (%)
0·2
0·1
0
0
20
40
60
80
100

The attainable vibrational temperature of a N_2-He mixture is much greater than that of a CO_2-He mixture for a given belium content. Therefore, during the discharge in a ternary mixture of CO_2-N_2-He, the vibrational temperature of the ν_3 mode CO_2 molecules is different than that of the N_2 molecules. Subsequently, the rapid V-V energy exchange brings these two resonant modes into equilibrium. As for a given He content, the excitation rates to different levels of CO_2 and N_2 are approximately constant, the total ν_3 mode vibrational energy in a ternary mixture (provided $X_{CO_2} + X_{N_2}$ constant) is therefore equal to the linear combination of the total ν_3 mode vibrational energy in a N_2-He mixture and a CO_2-He mixture with coefficients X_{N_2} and X_{CO_2} respectively. The linear relationship between the total ν_3 mode vibrational energy and the mixture ratio $X_{CO_2}/(X_{CO_2} + X_{N_2})$ as observed in Fig. 15 confirms the above mechanism.

In summary, N_2 molecules are effectively excited in a glow discharge and can attain a vibrational temperature much higher that that of CO_2 molecules. Although the N_2 molecules cannot lase, they constitute an energy reservoir for the ν_3 mode levels of CO_2 through the rapid V-V energy exchange. For CO_2, the ineffectiveness of discharge excitation to the ν_3 mode at high input energies, and the low saturation level of the ν_3 mode vibrational energy are the principal causes for gain limitation in a TE CO_2 laser amplifier.

IV-3 Conclusions

The method used to investigate the gain limitation in TE CO_2 laser amplifiers is simple, and represents a great improvement over

previous methods [5,10,15] which relied on a theoretical fit to the measured gain of regular bands, with several adjustable parameters. The theoretical fit is insensitive to the absolute population of the laser levels [10].

In the present study, the combination of gain measurements on both the sequence and regular bands clearly demonstrates the existence of some de-excitation mechanism such as electron de-excitation, which reduces substantially the pumping efficiency to the ν_3 mode at increasing input energy. It is therefore necessary to incorporate the de-excitation mechanism of ν_3 mode excited states into the accurate modeling of CO_2 laser dynamics.

CHAPTER V

COMPARISON OF THEORETICAL MODEL WITH EXPERIMENTAL DATA

Now that the characteristic rotational and vibrational temperatures appropriate to TE CO_2 laser amplifiers can be determined from gain measurements of sequence, hot and regular laser bands, we are in a position to predict the small-signal gain with no variable parameters. Such a direct calculation (i.e. with no variable parameters) is possible for the first time, as opposed to previous works in which the vibrational temperatures were not known experimentally, and were taken as variable parameters. A comparison of the calculated gain with experimental data is a good test of the agreement between our measurements and the conventional "mode temperature" treatments.

V-1 Inputs for gain calculation

Three temperatures, namely, rotational temperature T_R, ν_3 mode vibrational temperature T_3, ν_2 and ν_1 mode vibrational temperature, T_2, are required for the gain calculation.

(a) Rotational temperature T_R

As outlined in Section II-5.3, the rotational temperature is derived from the gain distribution of rotational lines. This procedure is applied to the 9.4 μm $00^0 1$ P-branch rotational lines measured at gain peak. Typical results are illustrated in Fig. 16, and the accuracy

FIGURE 16

Typical gain distribution of rotational lines used for derivation of rotational temperature T_R in the discharge. Circles represent experimental measurements, and typical errors bars are shown. The dashed and solid lines indicate the calculated gain distribution for two different rotational temperatures. Note that the relative gain of rotational lines of high J-value (i.e. $J \geq 28$) is more sensitive to changes in temperature than that of low J-value.

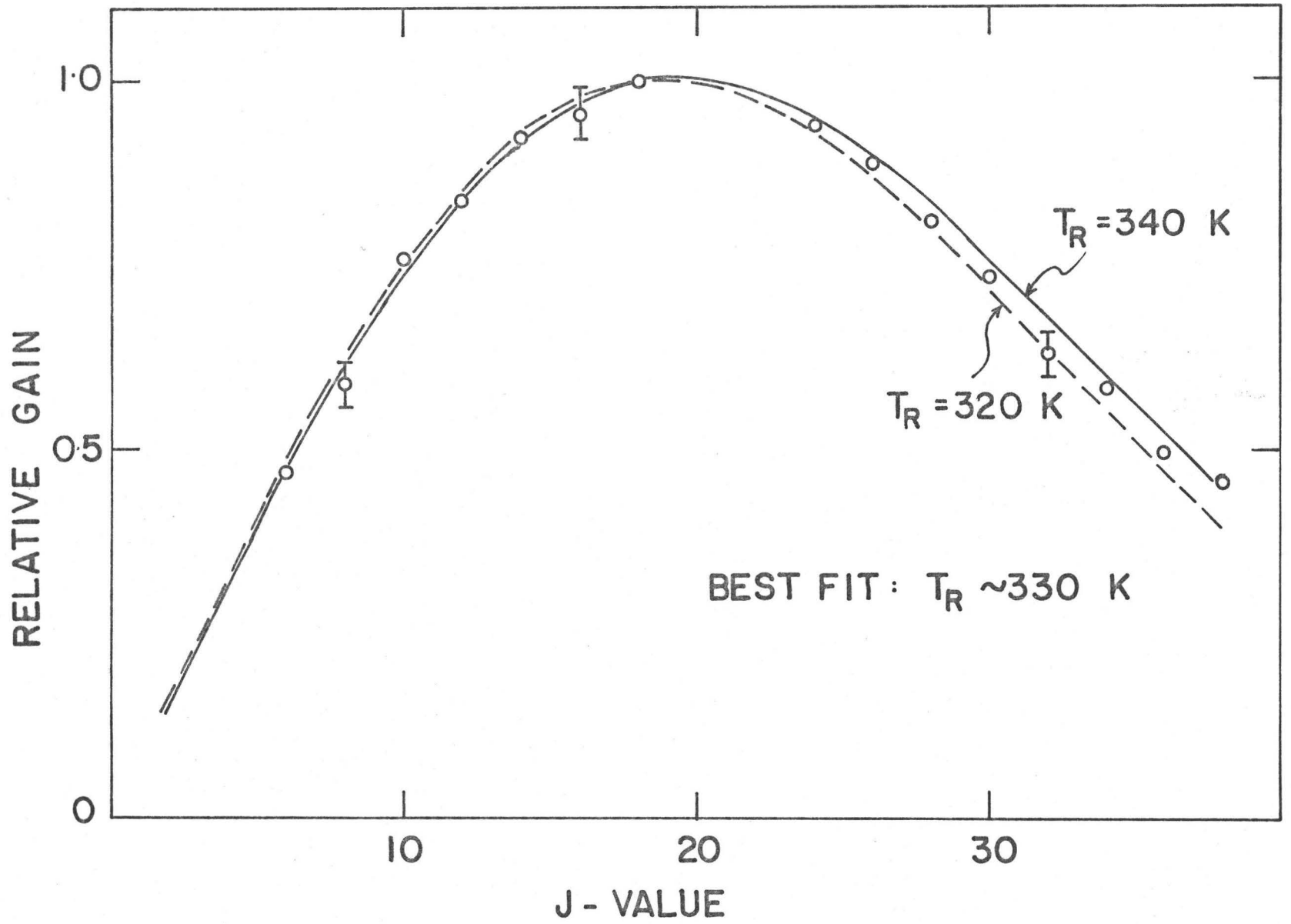
1·0
0·5
0
RELATIVE GAIN
10
20
30
J - VALUE
T_R =340 K
T_R =320 K
BEST FIT : T_R ~330 K

of the derived temperature is ~±10 K. The rotational temperature measured as a function of input energy is shown in Fig. 17 for the 13% CO_2:10% N_2:77% He mixture, and in Fig. 18 for the 3% CO_2:97% He mixture. It can be seen that the rotational temperature increase is modest, and T_R is only 400 K at ~400J/ℓ-atm for the 13% CO_2 mixture. The temperature increase is even smaller for the 3% CO_2 mixture due to higher He content in this mixture. The linear increase of rotational temperature with input energy is expected from simple thermodynamic considerations (see Appendix B).

(b) ν_3 mode vibrational temperature T_3

The vibrational temperature T_3 is derived from the measured gain ratio of the sequence band to the regular band (as outlined in Section II-5.1). The variation of T_3 with input energy is shown in Fig. 17 for the 13% CO_2 mixture, and in Fig. 18 for the 3% CO_2 mixture. The saturation of T_3 at high input energies is evident for both mixtures. The data points for T_3 shown in Figs. 17 and 18 are obtained from the best fit line to the measured gain ratios and the accuracy of T_3 is estimated to be ±80 K.

(c) ν_2 mode vibrational temperature T_2

Two different methods are used to estimate the ν_2 mode vibrational temperature. The first one is based on the measured gain ratio of the hot band to the regular band (as outlined in Section II-5.2). This method is direct but not very accurate due to the weak gain of the hot band and the low intensity of the probe beam. The method is

FIGURE 17

Variation of temperatures T_3, T_2 and T_R with input energy for a 13% CO_2:10% N_2:77% He mixture. For the temperature T_2, Δ represent the results obtained from gain measurements of the hot band and O give results from an alternative method (see text)

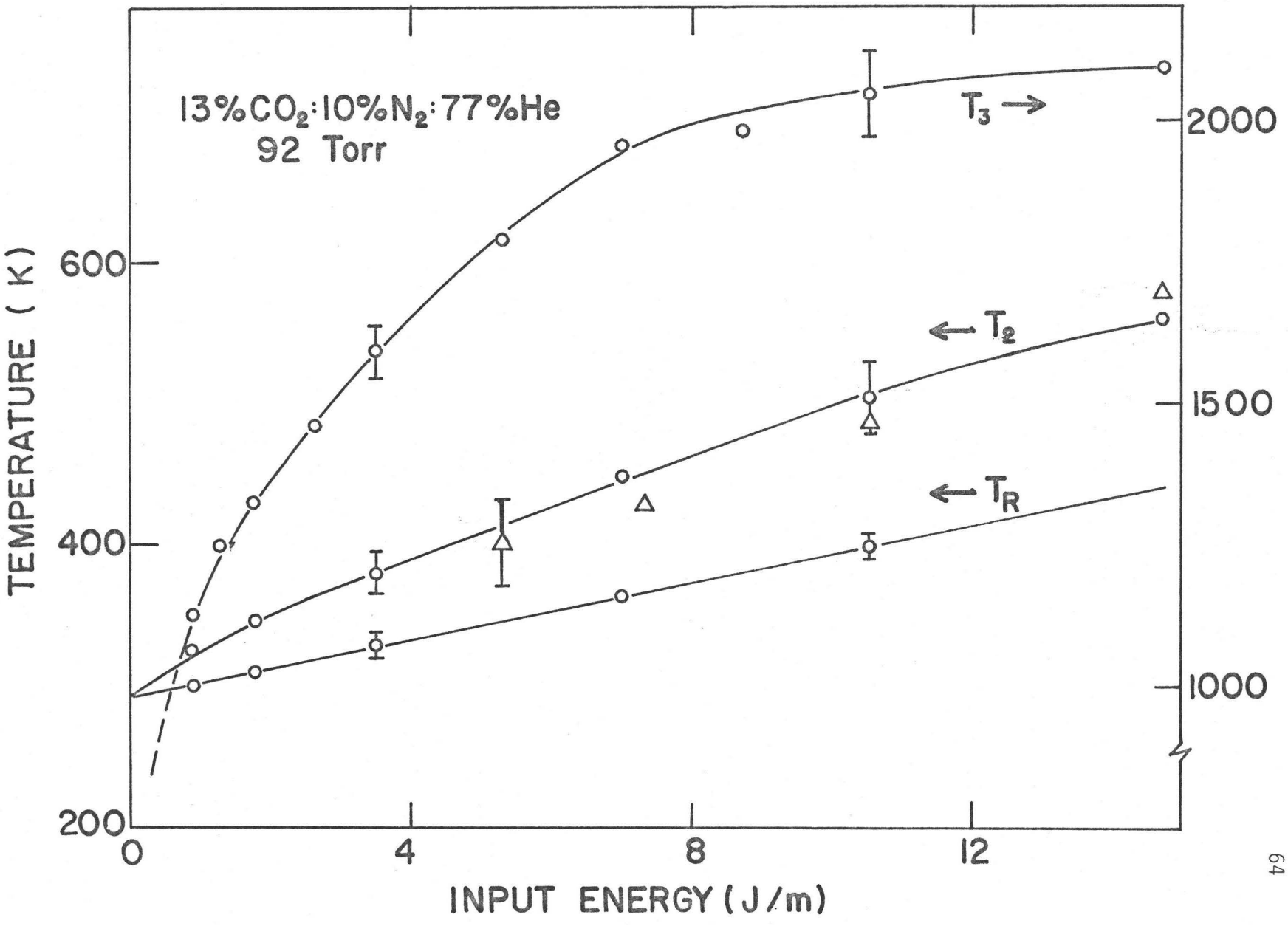
13%CO2:10%N2:77%He
92 Torr
T3 →
← T2
← TR
TEMPERATURE (K)
200
400
600
1000
1500
2000
0
4
8
12
INPUT ENERGY (J/m)

FIGURE 18

Variation of temperatures T_3, T_2 and T_R with input energy for a 3% CO_2:97% He mixture. Experimental points are shown by O.

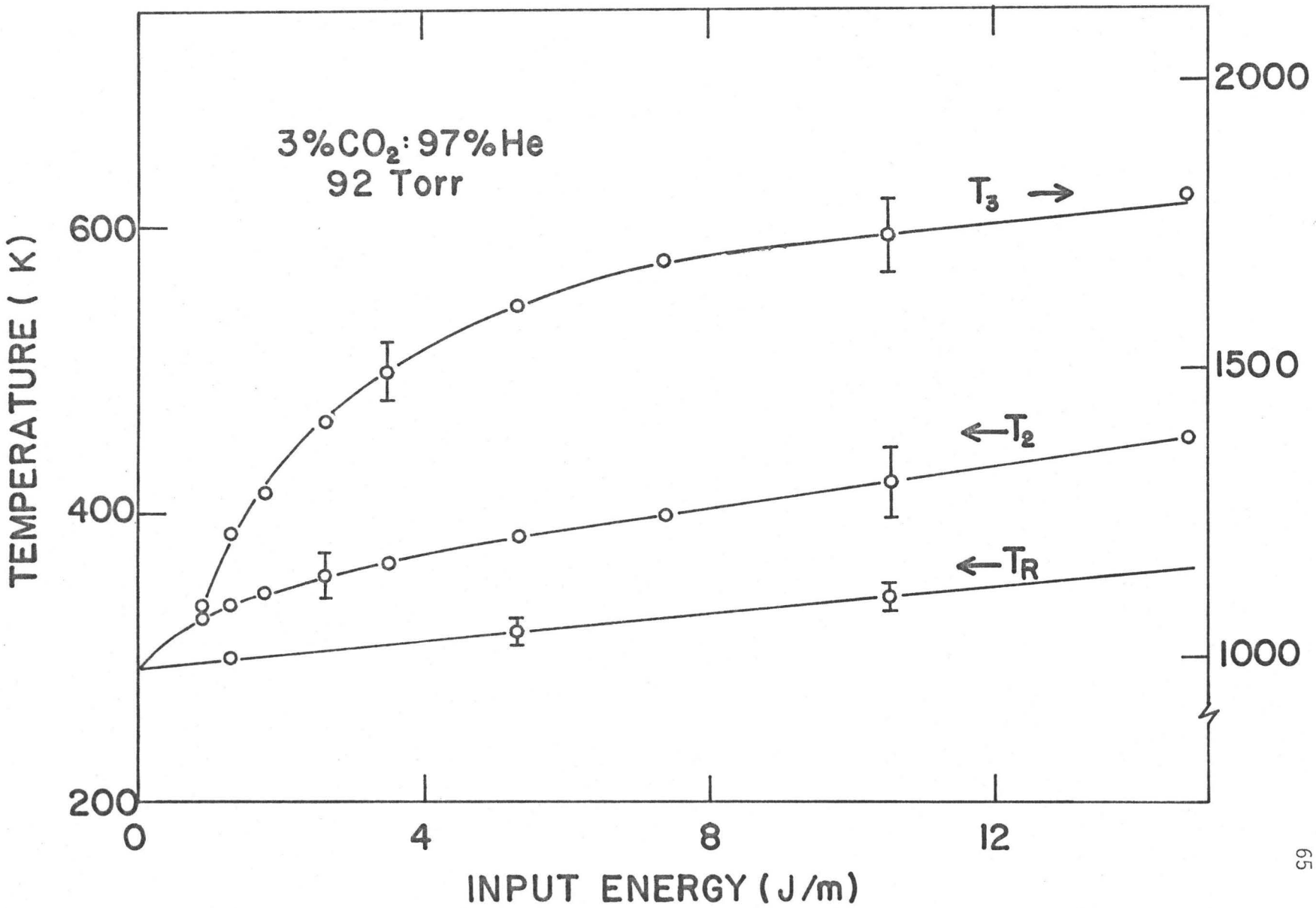
3%CO2:97%He
92 Torr
T3 →
←T2
←TR
TEMPERATURE (K)
600
400
200
2000
1500
1000
0
4
8
12
INPUT ENERGY (J/m)

particularly poor for low values of T_2 and is used only at high input energy where the gain of the hot band can be measured with reasonable accuracy. The accuracy of T_2 by this method is estimated to be $\sim\pm 30$ K. A second method based on the balance of relaxation rates between the upper and lower laser level populations at gain peak is presented in Appendix C. This second method has an accuracy comparable to the first one and is applicable to both low and high input energies. The results from both methods are in good agreement (as shown in Fig. 17). As can be seen from Figs. 17 and 18, the temperature T_2 is not high and does not deviate very much from the rotational temperature T_R. Therefore, T_2 does not have a strong effect on the gain. This is expected from the rapid relaxation of the lower laser levels [11].

In all the gain calculations, we have assumed that the ν_1 mode temperature, i.e. T_1, is identical to T_2. Some experiments [18,58] suggest that ν_1 and ν_2 modes may not be in equilibrium. This implies that T_1 is different than T_2. However, the gain of 9.4 μm bands is insensitive to T_1, and the difference between T_1 and T_2 has negligible effect on the gain calculations of the 9.4 μm bands.

The variation of the measured T_R, T_3 and T_2 temperatures as a function of input energy shown in Figs. 17 and 18 are the inputs for the gain calculations.

V-2 Results and discussions

The results of gain calculations for the two mixtures, 13% CO_2 and 3% CO_2, are displayed in Figs. 19 and 20 by the solid lines. The experimental data are shown in the same figures by the open circles.

FIGURE 19

Comparison between calculated gain and experimental data for a 13% CO_2: 10% N_2:77% He mixture at 92 torr. The solid line represents the gain values calculated with molecular constants in Table I. The dashed line is obtained from the solid line multiplied by a scaling factor of 0.83 (see text). O are the experimental points.

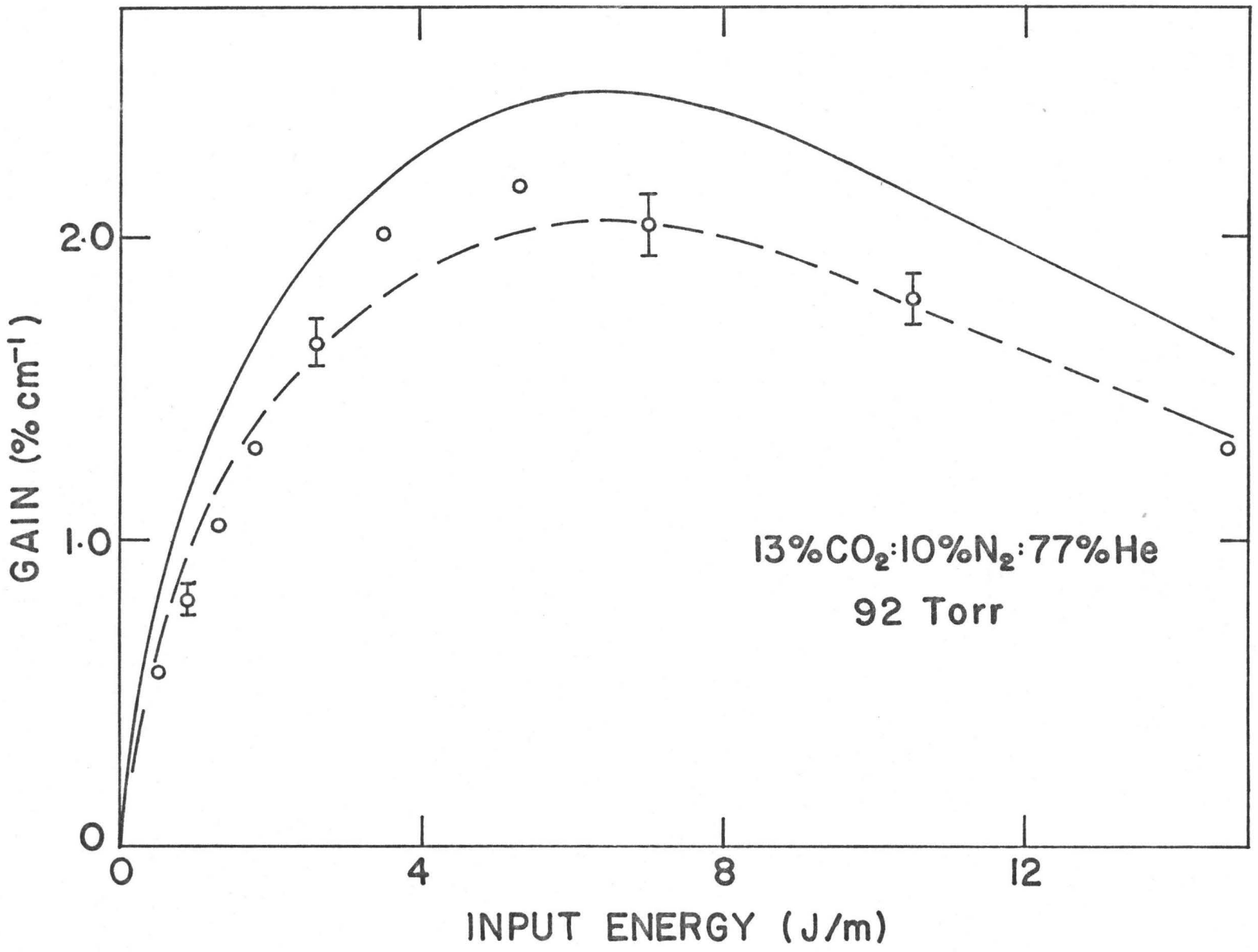
GAIN (% cm⁻¹)
2·0
1·0
0
0
4
8
12
INPUT ENERGY (J/m)
13%CO₂:10%N₂:77%He
92 Torr

FIGURE 20

Comparison between calculated gain and experimental data for a 3% CO_2: 97% He mixture at 92 torr. The solid line represents the gain values calculated with molecular constants in Table I. The dashed line is obtained from the solid line using the same scaling factor as in Fig. 19. O are the experiment points.

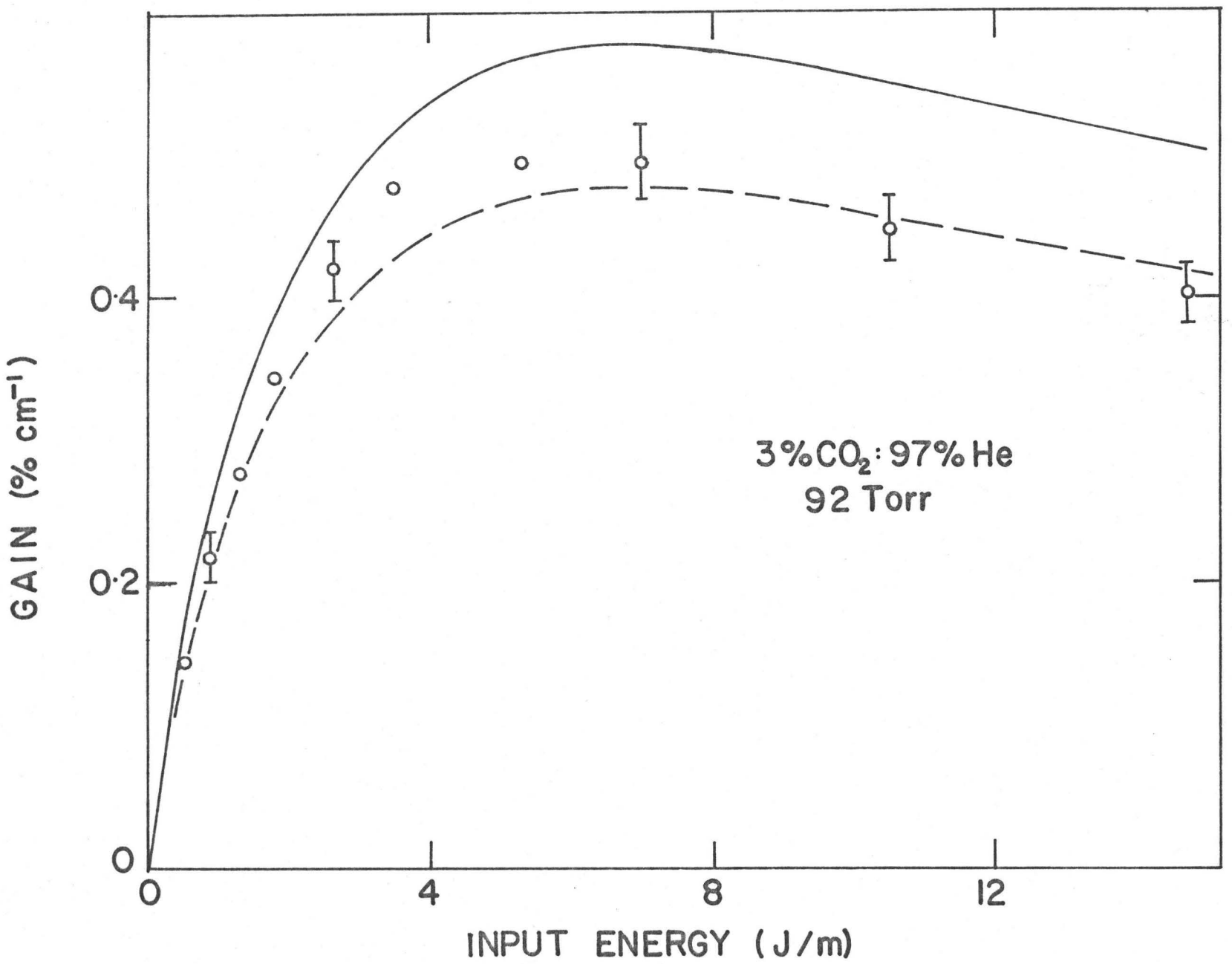
GAIN (% cm⁻¹)
0·4
0·2
0
0
4
8
12
INPUT ENERGY (J/m)
3%CO₂: 97% He
92 Torr

Clearly, from Figs. 19 and 20, the general trend of the calculated gain is in good agreement with that of the experimental data for both mixtures over the entire range of input energies. There is, however, a constant ~20% discrepancy between the calculated and experimental values. We have therefore scaled all the calculations by a constant factor of 0.83. The scaled values of gain are represented by the dashed lines in Figs. 19 and 20 (A constant scaling factor of this nature can easily be justified by uncertainties in the input data to the gain calculations, as discussed in Appendix D). Excellent agreement between calculation and experiment is now obtained for both mixtures over the entire range of input energies, confirming that the gain behavior (i.e. rapid initial increase, then saturation and fall of gain) versus input energy is dominated by the saturation of T_3. This agreement between calculation and experiment confirms the accuracy of our vibrational and rotational temperatures measurements at both low and high input energies.

V-3 Conclusions

In this chapter, we have shown that the absolute value of the gain of the 9.4 μm regular bands calculated from Eq. (4) using the three measured temperatures T_R, T_3 and T_2, agrees well with the experimental gain provided a constant scaling factor is used to account for uncertainties in the linestrengths and linewidths of the 9.4 μm bands. The good agreement between theory and experiment obtained for two very different mixtures, and over a wide range of input energies, confirms that the conventional "mode temperature" model for CO_2 laser dynamics is valid

and that the saturation of ν_3 mode vibrational temperature, T_3, is mainly responsible for the limitation of gain in TE CO_2 laser amplifiers. Thermal effects play only a secondary role.

CHAPTER VI

CONCLUSIONS

In this chapter, we outline the important conclusions that can be drawn from the work reported in this thesis. As detailed in Chapter I, the gain limitation with increasing input energy places an upper limitation on the extraction of optical energy from a TE CO_2 amplifier. The work in this thesis was aimed at demonstrating the existence of a de-excitation mechanism responsible for the observed gain limitation with increasing input energy. The novel technique used for direct determination of characteristic temperatures relevant to the CO_2 discharge has proven to be an accurate and powerful technique for detailed investigation of CO_2 laser dynamics. The results reported in this thesis establish strong experimental evidence which have made the present work successful in its aim. All the important conclusions are covered in Chapters IV and V; the present chapter is concerned with giving a brief account of the overall significance of the research. Seven major points are summarized below:

(1) The saturation of ν_3 mode vibrational temperature, T_3, at high input energies is the principal cause for gain limitation in a TE CO_2 laser amplifier (see Section IV-2).

(2) In contrast to the conclusions of previous researchers, we find that thermal effects play only a secondary role for gain

limitation in TE CO_2 laser amplifiers (see Section V-1).

(3) The population of the lower laser level is always small compared to that of upper laser level at the time of gain peak. This is consistent with fast relaxation of the lower laser levels (see Section V-1).

(4) The N_2 molecules are very effectively excited in a glow discharge, and the attainable vibrational temperature is much higher than that of the ν_3 mode of CO_2 molecules (see Section IV-2.c).

(5) The vibrational levels of N_2 are strongly coupled to the ν_3 mode levels of CO_2, and constitute an energy reservoir for the ν_3 mode (see Section IV-2.c)

(6) The absolute value of gain calculated with the three measured temperatures is in good agreement with the experimental data. Such a direct comparison confirms the validity of the conventional "mode temperature" model for CO_2 laser dynamics and strongly supports our findings that the gain limitation is dominated by the saturation of T_3 (see Section V-2).

(7) The reduction of pumping efficiency to the ν_3 mode with increasing input energy is due to a de-excitation mechanism occurring in the glow discharge (see Section IV-2.b).

The above conclusions are strongly supported by direct experimental evidence and lead to a better understanding of the CO_2 laser dynamics. Further investigations are needed for detailed understanding of the de-excitation mechanism. Previous experiments [21,22] have shown that the electron de-excitation rate of excited

states is many times greater than the electron excitation rate in a CO_2 discharge. An exact knowledge of this de-excitation rate is of primary importance for understanding the dynamics of the laser system. Hence, the next step in developing an accurate model of CO_2 laser dynamics is to measure such de-excitation rate.

Another important experimental extension of the present work would be the investigation of the population dynamics in various high lying vibrational levels. Such an investigation will provide precise information on many important processes occurring in the CO_2 molecules and between CO_2 and other molecular species. Also, these measurements will give a crucial test on the validity of the "vibrational mode temperature" model for CO_2 laser dynamics.

APPENDIX A

INPUT ENERGY

To calculate the input energy per unit volume to the gas, we must know the exact amount of energy coupled into the gas, and the energy distribution in the discharge volume. The energy into the gas can be measured from the voltage-current characteristics of the discharge; the discharge volume is estimated from the spatial distribution of gain at low discharge energy across the amplifier [10].

In the present study, the input energy is simply obtained from the ratio of capacitor stored energy to discharge length, and has units of Joule/meter. This simple unit is convenient and adequate for the present experiment. In fact, none of the conclusions established from experiment depend on the absolute value of input energy. However, to calculate the pumping efficiency and to facilitate the comparison with other works, this simple unit has to be converted into the commonly used unit, i.e. Joule/liter-atm, with the losses of discharge circuit,and the discharge volume,being taken into account. For this purpose, we compare the variation of gain versus input energy for the 3% CO_2:97% He mixture to that of Ballik et al for the same mixture[10] where the input energy was expressed in J/l-atm. A conversion factor between the two units (i.e. J/l to J/l-atm) is obtained for the 3% CO_2:97% He mixture. This is possible because the energy into the gas is linearly

proportional to the capacitor stored energy (this is justified by the measurements of absorption temperature. See Appendix B), and the discharge volume remains constant with input energy [10]. The conversion factor varies with mixture, and a rough estimation of this conversion factor for other mixtures is obtained from the work of Robinson [5] by assuming a linear relationship between the discharge efficiency (as defined in the above reference) and the He content. The conversion factors are summarized in Table IV.

We can now calculate the pumping efficiency to ν_3 mode from the ratio of total ν_3 mode vibrational energy to the input energy. That is:

$$\varepsilon(\nu_3) = \frac{(X_{CO_2}+X_{N_2})\ \frac{P_o V_e}{k_B T_o}\ h\nu_3 \left(\frac{x_3}{1-x_3}\right)_{t=0}}{E_e} \qquad \text{(A-1)}$$

Where X_{CO_2}, X_{N_2} are the factional composition of CO_2 and N_2 in the gas mixture; P_o is the total static pressure; T_o is the room temperature ($\sim$294 K); V_e is the discharge volume, E_e is the input energy into the gas.

Equation (A-1) can be rewritten as:

$$\varepsilon(\nu_3) = \frac{h\nu_3}{k_B T_o} \frac{(X_{CO_2}+X_{N_2})\left(\frac{x_3}{1-x_3}\right)_{t=0}}{(E_e/P_o V_e)}$$

$$= 1165 \frac{(X_{CO_2}+X_{N_2})\left(\frac{x_3}{1-x_3}\right)_{t=0}}{(E_e/P_o V_e)} \qquad \text{(A-2)}$$

where $(E_e/P_o V_e)$ is the input energy in unit of J/l-atm.

TABLE IV

CONVERSION FACTORS FROM J/m TO J/l-atm

Mixture CO_2: N_2: He	Conversion factors for the present system
3%: 0%: 97%	1 J/m → 28.6 J/l-atm (a)
13%: 10%: 77%	1 J/m → 36.3 J/l-atm (b)
3% : 21%: 76%	1 J/m → 36.3 J/l-atm (b)

(a) Ballik *et al* [10]

(b) Rough estimate (± 10%) from data of Robinson [5].

APPENDIX B

INCREASE OF GAS TEMPERATURE WITH INPUT ENERGY

From simple thermodynamic considerations, the increase of kinetic temperature (or gas temperature) at constant volume is proportional to the amount of heat (or energy) added to the gas, i.e.

$$\Delta T = \frac{Q}{nC_v'} \qquad \text{(B-1)}$$

where ΔT is the increase of temperature; Q is the energy added to the gas; n is the number of moles of gas and C_v' is the molar heat capacity of the gas at constant volume.

For a gas mixture of CO_2, N_2 and He with n_c mole of CO_2, n_N mole and N_2 and n_H mole of He, we have:

$$\Delta T = \frac{Q}{n_c C_v'(CO_2) + n_N C_v'(N_2) + n_H C_v'(He)} \qquad \text{(B-2)}$$

where $C_v'(CO_2)$, $C_v'(N_2)$ and $C_v'(He)$ are the molar heat capacity of CO_2, N_2 and He respectively.

Using the ideal gas law, Eq. (B-2) can be written as:

$$\Delta T = \left(\frac{Q}{P_o V_o}\right) \frac{RT_o}{[X_{CO_2} C_v'(CO_2) + X_{N_2} C_v'(N_2) + X_{He} C_v'(He)]} \qquad \text{(B-3)}$$

where P_o is the total pressure; V_o is the volume of gas; T_o is the initial gas temperature; X_{CO_2}, X_{N_2}, X_{He} are the fractional composition of CO_2, N_2 and He respectively in the mixture and R is the gas constant.

The increase of gas temperature following the gain peak is due to the relaxation of vibrational energies. The transmittance of the probe beam measured at the end of the gain pulse allows us to determine the gas temperature at that time [5,73]. Figure 21 shows a plot of gas temperature measured at gain peak and at absorption peak as a function of input energy for a 13% CO_2:77% N_2:77% He mixture. The linear increase of gas temperature with input energy is expected from Eq. (B-2), and confirms that the input energy to the gas is directly proportional to the stored energy in the capacitors.

FIGURE 21

Increase of gas temperature with input energy in a discharge of 13% CO_2:10% N_2:77% He mixture at 92 torr. Δ are measurements derived from rotational distribution at gain peak, and O represent temperatures derived from absorption measurements following the gain pulse. The substantial difference between temperature at absorption peak and temperature at gain peak is due to the relaxation of vibrational energies into kinetic energy.

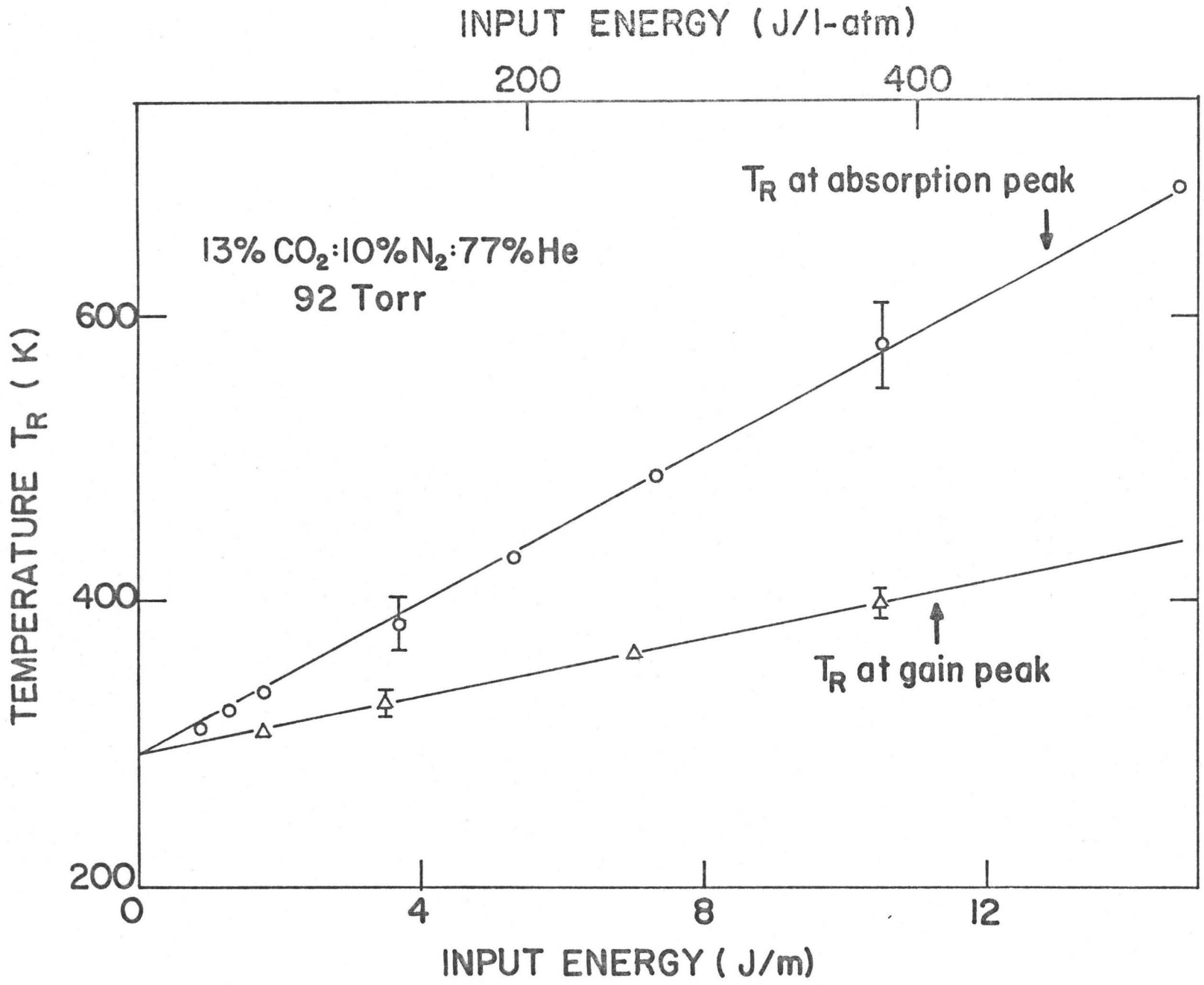
INPUT ENERGY (J/l-atm)
200
400
T_R at absorption peak
13% CO_2:10% N_2:77% He
92 Torr
600
400
200
TEMPERATURE T_R (K)
T_R at gain peak
0
4
8
12
INPUT ENERGY (J/m)

APPENDIX C

DERIVATION OF TEMPERATURE T_2 FROM THE GAIN PULSE

The small-signal gain α is proportional to the difference of population between the upper and lower laser levels, i.e. $N_u - N_\ell$. At the time of gain peak, the derivative of α is zero, hence we have:

$$\frac{d(N_u - N_\ell)}{dt} = 0 \qquad \text{(C-1)}$$

or $$\frac{dN_u}{dt} = \frac{dN_\ell}{dt}$$

or $$\frac{N_u - N_u^e}{\tau_u} = \frac{N_e - N_\ell^e}{\tau_\ell}$$

Where N_u, N_ℓ are the populations of the upper and lower laser level at gain peak; N_u^e, N_ℓ^e are the populations of the upper and lower laser level at equilibrium with gas temperature at time of gain peak; τ_u, τ_ℓ are the relaxation times of the upper and lower laser level [69].

For the gain pulse of transition $00^0 1$-$02^0 0$ P(18), we have at the gain peak:

$$N_{02^0 0}(T_2) = N^e_{02^0 0}(T_R) + \frac{\tau_{02^0 0}}{\tau_{00^0 1}} \left[N_{00^0 1}(T_3) - N^e_{00^0 1}(T_R)\right] e^{-21.70/T_R} \qquad \text{(C-2)}$$

where the nomenclature of Chapter II is used and the exponential factor in Eq. (C-2) arises from an exact treatment of the rotational distribution.

$\tau_{02^0_0}$ is measured from the rise time of the gain pulse and is almost constant irrespective of the input energy. $\tau_{00^0_1}$ is measured from the fall time of the gain pulse and varies with input energy. The temperatures T_R and T_3 are also measured (see Section V-1). The only unknown T_2 is derived from Eq. (C-2).

APPENDIX D

DISCUSSION ON THE SCALING FACTOR USED IN CHAPTER V

In Chapter V, a constant scaling factor was used in the gain calculations to improve agreement with experimental data. As this scaling factor is the same for two very different gas mixtures and remains constant at both high and low input energies, the discrepancy between calculation and experiment cannot be caused by any energy or temperature dependent processes. Hence we can rule out CO formation (this will lower the experimental gain at high input energies) and under-estimation of T_2 and T_R (this will not affect the fitting at low input energies). However, our calculated gain is very dependent on the values of the linestrength and linewidth of the regular band (as measured previously by others [41,43]) and the ratio $\left|R_{02^0 1}^{00^0 2}\right|^2 / \left|R_{02^0 0}^{00^0 1}\right|^2$ (as measured by Reid [46]). Any uncertainty in these values will lead to a constant scaling factor in the gain calculations. Furthermore, as we can measure T_R and T_2, the temperature T_3 can also be derived from the absolute value of the measured regular gain by using Eq. (4). The value of T_3 deduced from this method is constantly lower by $\sim+150^{\circ}K$ than the value obtained from the gain ratio of sequence to regular bands. This has also been observed by Lavigne et al. [72] and is a further evidence that the values of the linestrength and linewidth of the 9.4 μm regular band, and the ratio

$\left|R^{00^o2}_{02^o1}\right|^2 / \left|R^{00^o1}_{02^o0}\right|^2$ are possible sources of discrepancy between the calculated gain and the experimental data.

REFERENCES

[1] A.J. Beaulieu, Appl. Phys. Lett. 16, 504 (1970).

[2] V.S. Letokhov, C.B. Moore, Sov. J. Quantum Electron., Vol. 6, No. 2, 129 (1976) and No. 3, 259 (1976).

[3] R.V. Ambartzumian, G.N. Makarov and A.A. Puretzby, Optics Letters, Vol. 3, 103 (1978).

[4] G.K. Anderson and J.T. Lee, Optics Letters, Vol. 3, 10 (1978).

[5] A.M. Robinson, Can. J. Phys., 50, 2138 (1972) and 247 (1972).

[6] H.G. Ahlstrom, A.L. Pindroh, J. Holzrichter, T. Kan, G. Inglesakis, A.C. Kolb and H.J. Jansen, IEEE J. Quantum Electron. QE-10, 26 (1974).

[7] A.M. Robinson, J. Appl. Phys., Vol. 47, No. 2, 608 (1976).

[8] H.J.J. Seguin, K.H. Nam and J. Tulip, IEEE J. Quantum Electron., QE-15, 44 (1979) and 50 (1979).

[9] J.M. Hoffman, F.W. Bingham and J.B. Moreno, J. Appl. Phys., 45, 1798 (1974).

[10] E.A. Ballik, B.K. Garside, J. Reid and T.Tricker, J. Appl. Phys., 46, 1322 (1975).

[11] B.K. Garside, J. Reid and E.A. Ballik, IEEE J. Quantum Electron., QE-11, 264 (1975).

[12] R.H. Bullis, W.L. Nighan, M.C. Fowler and W.J. Wiegand, AIAA Journal, Vol. 10, No. 4, 407 (1972).

[13] L.J. Denes and J.J. Lowke, Appl. Phys. Lett., Vol. 23, No. 3, 130 (1973).

[14] L.E. Kline and L.J. Denes, J. Appl. Phys., Vol. 46, No. 4, 1567 (1975).

[15] L.J. Denes and L.A. Weaver, J. Appl. Phys., Vol. 44, No. 9, 4125 (1973).

[16] D. Bailly, D. Gaultier, C. Rossetti et P. Barchewitz, Can. J. Phys., 50, 2605 (1972).

[17] G. Girard, M. Huguet and M. Michon, IEEE J. Quan. Elec. QE-9, 426 (1973).

[18] E.R. Murray, C.H. Kruger and M. Mitchner, J. Chem. Phys. Vol. 62, No. 2, 388 (1975).

[19] J. Reid and K. Siemsen, Appl. Phys. Lett., Vol. 29, No. 4, 250 (1976).

[20] J. Reid and K. Siemsen, J. Appl. Phys., Vol. 48, No. 7, 2712 (1977).

[21] B.M. Christophe and A.A. Offenberger, Can. J. Phys. 50, 368 (1972).

[22] M.C. Gower and A.I. Carswell, Appl. Phys. Lett. 22, 321 (1973).

[23] A.R. Davies, K. Smith and R.M. Thomson, J. Appl. Phys., Vol. 47, No. 5, 2037 (1976).

[24] All the properties and equations discussed in this chapter are only true for the $C^{12}O_2^{16}$ isotope molecule, but because it occurs at a natural abundance of 98.4%, the other isotopic molecules have negligible effect on the laser characteristics.

[25] G. Herzberg, "Infared and Raman spectra," Van Nostrand Co., Princeton, 1945.

[26] P.K. Cheo, "CO_2 lasers" in Lasers, Vol. 3, A.K. Lerine and A.J. Demaria, eds. (Marcel Dekker, Inc., New York, 1971).

[27] C.K.N. Patel, Phys. Rev. 136A, 1187 (1964).

[28] Some authors use the $[10^0 0, 02^0 0]_{I, II}$ notation (where I stands for 10.4 μm) to emphasize the Fermi resonance of two lower laser levels, however the notation in the text is retrained for its simplicity and its obvious distinction.

[29] The intensity anomalies arise from the overlapping of two closely spaced transitions. See Reference [30].

[30] S.A. Munjce and W.H. Christiansen, Applied Optics, Vol. 12, No. 5, 993 (1973).

[31] W. Berger, K. Siemsen and J. Reid, Rev. Sci. Instrum., Vol. 48, No. 8, 114 (1977).

[32] In all parts of this thesis, the "gain coefficient" or "gain" means the small-signal gain, i.e., gain with no intensity saturation.

[33] A.M. Robinson, "Computed absorption coefficient for CO_2 laser transitions", report TN-1989/71, Defence Research Establishment Valcartier, Quebec, Canada.

[34] T.J. Bridges and T.Y. Chang, Phys. Rev. Lett., 22, 811 (1969).

[35] J. Dupre-Maquaire and P. Pinson, J. Mol. Spectros., 62, 181 (1976).

[36] S.S. Penner, "Quantitative molecular spectroscopy and gas emissivities", Addison-Wesley Co.(1959).

[37] R.R. Patty, E.R. Manring and J.A. Gardner, Appl. Opt., 7, 2241 (1968).

[38] R. Ely and T.K. McCubbin, Appl. Opt., 9, 1230 (1970).

[39] A.M. Robinson and N. Sutton, Appl. Opt., 18, 378 (1979).

[40] J.L. Miller, J. Appl. Phys., 49, 3076 (1978).

[41] C. Cousin, C. Rossetti and C. Meyer, C.R. Acad. Sc. Paris, 268, 1640 (1969).

[42] E. Arié, N. Lacome and C. Rossetti, Can. J. Phys., 50, 1800 (1972).

[43] C. Young and R.E. Chapman, J.Q.S.R.T., 14, 679 (1974).

[44] R.L. Abrams, Appl. Phys. Lett., Vol. 25, 609 (1974).

[45] E.R. Murray, C. Kruger and M. Mitchner, Appl. Phys. Lett., Vol. 24, No. 4, 180 (1974).

[46] J. Reid, J. Shewchun and B.K. Garside, Appl. Phys., 17, 349 (1978).

[47] K.J. Siemsen: Private communication.

[48] L.S. Rothman and W.S. Benedict, Appl. Opt., 17, 2605 (1978).

[49] L.D. Gray and J.E. Selvidge, J.Q.S.R.T., Vol. 5, 291 (1965).

[50] In calculating Q_{int}, the electronic partition function is taken to be unity, since the first electronic excited state of CO_2 lies far above the ground state. At low excitation, almost all the CO_2 molecules are in the electronic ground state.

[51] The absorption coefficient is defined as the negative value of the gain coefficient in Eq. (4).

[52] B.F. Gordietz, N.N. Sobolev, V.V. Sokovikov and L.A. Shelepin, IEEE J. Quantum Electron., Q.E.4, No. 11, 796 (1968).

[53] C.B. Moore, R.E. Wood, B.L. Hu and J.T. Yardley, J. Chem. Phys., Vol. 46, 4222 (1967).

[54] J. Tulip, IEEE J. Quan. Elec., 6, 206 (1970).

[55] K.R. Manes and H.J. Seguin, J. Appl. Phys., Vol. 43, No. 12, 5073 (1972).

[56] L.O. Hocker, M.A. Kovacs, C.K. Rhodes, G.W. Flynn and A. Javan, Phys. Rev. Lett., 17, No. 5, 233 (1966).

[57] W.A. Rosser Jr., A.D. Wood and E.T. Gerry, J. Chem. Phys., Vol. 50, 4996 (1969) and Vol. 51, 2286 (1969).

[58] W.A. Rosser Jr., E. Hoag and E.T. Gerry, J. Chem. Phys., Vol. 57, 4153 (1972).

[59] T.A. Detemple, D.R. Suhre and P.D. Coleman, Appl. Phys. Lett., Vol. 22, No. 8, 849 (1973).

[60] E.E. Stark Jr., Appl. Phys. Lett., Vol. 23, No. 6, 335 (1973).

[61] P.K. Cheo, Appl. Phys. Lett., Vol. 14, 47 (1969).

[62] In calculating $E_3(T_3)$, we assume that the vibrational energy quanta is the same for CO_2 and N_2.

[63] L.A. Weaver, L.H. Taylor and L.J. Denes, Vol.46, No. 9, 3951 (1975).

[64] R.L. Taylor and S. Bitterman, Rev. Mod. Phys., Vol. 41, No. 1, 26 (1969).

[65] O.R. Wood, Proc. IEEE 62, 355 (1974), and cited references.

[66] R. Fortin, M. Gravel and R. Tremblay, Can. J. Phys. 49, 1783 (1971).

[67] R.R. Jacobs, Rev. Sci. Instrum. 44, 1146 (1973).

[68] The gain ratio between two laser bands has a weak dependence on the rotational temperature through the Boltzmann factor. This dependence is minimised for two lines of same rotational quantum number.

[69] P.K. Cheo, J. Appl. Phys. 38, 3563 (1967).

[70] J.J. Lowke, A.V. Phelps and B.W. Trwin, J.Appl. Phys., Vol. 44, No. 10, 4664 (1973).

[71] W.L. Nighan, Phys. Rev. A. 2, No. 5, 1989 (1970).

[72] P. Lavigne, J. L. Lachembre and G. Otis, J. Appl. Phys., Vol. 49, No. 7, 3718 (1978).

[73] A.M. Robinson and Y.K. Hsieh, J. Appl. Phys., Vol. 48, No. 4, 1589 (1977).

[74] The expression of $\Delta\nu_c$ in text is derived for the case with gas expansion. However, in short pulsed discharge system, the gas has a constant particle density in the discharge volume during the first hundred microseconds after the discharge as the gas has no time to expand. Therefore, the temperature dependence of $\Delta\nu_c$ becomes $T^{+\frac{1}{2}}$ instead of $T^{-\frac{1}{2}}$. However, this does not introduce changes in the values of gain at high pressure, because the value of particle density appears in both the numerator and denominator of the gain expression (Eq. 4).